ALEPH 94-178
PHYSIC 94-150
T. Oest
29 November 1994

A Measurement of the B^0 Lifetime using Partial Reconstructed Hadronic B^0 Decays

Thorsten Oest
CERN

Abstract

B^0 mesons were reconstructed with a new method using two pions $\pi_B^+\pi_D^-$ from a decay $B^0 \to \pi_B^+ X D^{*-}$, $D^{*-} \to D^0\pi_D^-$. 89 ± 10 B^0 were found in the 91-93 data. The main contributions are coming from the decays $B^0 \to \pi^+ D^{*-}$ and $B^0 \to \rho^+ D^{*-}$ with 36% and 27%, respectively. The B^0 lifetime was determined from an unbinned maximum likelihood fit to be

$$\boxed{\tau_{B^0} = 1.61\ ^{+0.22}_{-0.19}\ ^{+0.09}_{-0.07}\ ps}.$$

Chapter 1

Partial Reconstruction of Hadronic B^0 Decays

1.1 Introduction

Studies on B physics in general suffer from small branching rations to specific B decay channels. The efficiencies for a full reconstruction of an hadronic B decay is only of the order of 10^{-4}. Therefore semileptonic decays have widely been used to identify B hadrons. Although the partial reconstruction of these decays provides clean samples, the missing neutrino makes it difficult to distinguish between different B hadrons and to extract the momentum of the B meson.

An other method, not tried at LEP so far, is the partial reconstruction of hadronic B decays. The main idea is to look for decays of the type

$$\begin{aligned} B \;\rightarrow\; X \;\; & D^{*-} \\ & \rightarrow \pi_D^- D^0 \end{aligned} \tag{1.1}$$

without reconstructing the D^0. A reconstruction without knowledge on the D^0 momentum is possible because the π_D^- carries most of the information of the D^{*-} kinematics due to the small momentum transfer in the D^{*-} decay. Roughly speaking the D^{*-} momentum can be approximated as[1]:

$$\vec{p}_{D^*} \approx \frac{M_{D^*}}{M_\pi} \vec{p}_{\pi_D} \tag{1.2}$$

This idea has already been used to reconstruct hadronic [1, 2, 14] and semileptonic B^0 decays [3, 7] at $\Upsilon(4s)$ energies. Further applications are measurements of D^{*+} production in $e^+e^- \rightarrow c\bar{c}$ [4, 5, 6] and $\gamma\gamma \rightarrow c\bar{c}$ reactions[8]. Also note the possibility to apply the method to the decay $\Sigma_c \rightarrow \pi^- \Lambda_c^+$ [10].

In principal, the same method can be applied for decays with a D^{*0} or D_s^*. [2] Since the D^{*0} and D_s^* does not decay into a charged pion and a D meson which requires

[1] Or a little bit more precisely by $\vec{p}_{D^*} \approx \frac{M_{D^*}}{E'_\pi} \vec{p}_{\pi_D}$ where E'_π is the pion energy in the D^{*-} rest frame.

[2] The partial reconstruction of a D_s^* has been used at ARGUS to study the decay $B^0 \rightarrow D^{*-} D_s^{*+}$ [14].

a reconstruction of a π^0 or photon, we will concentrate only on decays including a D^{*-}. In addition the important constraint of a secondary B vertex can not be used for neutral particles.

In a spectator decay a charged D^{*-} can only be produced directly by a B^0. Measured branching ratios of such decays can be found in table 1.1. The method explained in this paper can therefore only be used to reconstruct B^0 mesons. On the first sight this seems to be a disadvantage, but on the other hand this also means that background from $B^{\pm}$, B_s or Λ_b decays is expected to be small.

Decay	BR	Γ_l/Γ	BR HVFL03
$B^0 \to \pi^+ D^{*-}$	(0.29 ± 0.16) % [13, 15] (0.23 ± 0.09) % [14] (0.40 ± 0.12) % [15] (0.26 ± 0.05) % [11]	100 %	
	(0.27 ± 0.04) %		0.30 %
$B^0 \to \rho^+ D^{*-}$	(0.6 ± 0.3) % [14] (1.9 ± 1.4) % [15] (0.74 ± 0.17) % [11]	(93 ± 7) % [11]	
	(0.72 ± 0.15) %		1.00 %
$B^0 \to a_1^+ D^{*-}$	(1.8 ± 0.8) % [15] (1.26 ± 0.15) % [11]		
	(1.28 ± 0.15) %		1.58 %
$B^0 \to \pi^+\pi^0 D^{*-} \Longrightarrow$ $B^0 \to (\pi^+\pi^0)_{non\ resonant} D^{*-}$	1.3 ± 0.4 % [14] 0.56 ± 0.43 %		2.26 %
$B^0 \to (\rho^0\pi^+)_{non\ resonant} D^{*-}$	0.68 ± 0.38 % [15]		1.74%
$B^- \to \pi^-\pi^- D^{*+}$	(0.24 ± 0.17) % [13, 15] (0.22 ± 0.13) %[14] (0.19 ± 0.08) %[11]		
	(0.20 ± 0.06) %		0.286 %
$B^- \to \pi^-\pi^-\pi^0 D^{*+}$	(1.5 ± 0.7) % [14]		0.51%
$B^- \to \pi^- D^{**0}(2420)$ $\to \pi^-\pi^- D^{*+}$	(0.07 ± 0.04) % [11]		
$B^- \to \pi^- D^{**0}(2460)$ $\to \pi^-\pi^- D^{*+}$	< 0.06 % @90%CL [11]		
$B^- \to \rho^- D^{**0}(2420)$ $\to \pi^-\pi^0\pi^- D^{*+}$	< 0.09 % @90%CL [11]		
$B^- \to \rho^- D^{**0}(2460)$ $\to \pi^-\pi^0\pi^- D^{*+}$	< 0.1 % @90%CL [11]		

Table 1.1: Branching ratios for hadronic B decays $B \to XD^{*-}$

1.2 The Reconstruction Method

Now we are going to explain the reconstruction technique. Once again, the aim is to extract the B^0 4-momentum from the reconstructed particles from the decay:

$$\begin{aligned} B^0 \;\rightarrow\; & X^+ \quad D^{*-} \\ & \rightarrow \pi_D^- D^0 \;. \end{aligned} \tag{1.3}$$

The D^0 will not be reconstructed. X^+ might be any system of particles. The simplest case is the decay $B^0 \rightarrow \pi^+ D^{*-}$. The B^0 4-momentum is needed in an analysis for different reasons:

- The B^0 **mass** or a related quantity can provide a signature for a B decay.
- The B^0 **direction of flight** is essential to suppress background since it must agree with the independent measurement by the jet direction and the B^0 decay vertex.
- The B^0 **momentum** must be known for the lifetime measurement.

1.2.1 Reconstruction of the Decay $B^0 \rightarrow X^+ D^{*-}$

The input for the reconstruction of the B momentum are the measured momenta p_{π_D} and p_X. Obviously the determination of the B^0 4-momentum is only possible in an approximation because the 4 degrees of freedom are reduced to 2 degrees of freedom by the constraints from the D^0 and D^{*-} mass. The simplest way to solve the kinematical problem is the scaling approximation $\vec{p}_{D^*} \approx m_{D^*}/m_\pi \cdot \vec{p}_{\pi_D}$, already mentioned above. This directly leads to the $X^+ D^{*-}$ mass and momentum.

A more precise approximation will be used here. To explain it, first let us concentrate on the extraction of the $X^+ D^{*-}$ invariant mass from the measured $X^+ \pi_D^-$ system. The B^0 mass is given by:

$$M_B^2 = M_{\pi X}^2 - M_D^2 + 2\; E'_B E'_D - 2\; |\vec{p}'_B||\vec{p}'_D| \cos\vartheta' \tag{1.4}$$

where the energies in the D^* rest frame are:

$$E'_B \;=\; \frac{M_B^2 + M_{D^*}^2 - M_X^2}{2M_{D^*}} \tag{1.5}$$

$$E'_D \;=\; \frac{M_{D^*}^2 + M_D^2 - M_\pi^2}{2M_{D^*}} \tag{1.6}$$

The uncertainty in a B^0 mass determination comes from the unknown D^{*-} decay angle ϑ'. The information on the $D^{*+}X$ mass which can be obtained from the $\pi_D^+ X$ system can only depend on the mass of the $\pi_D^+ X$ system. Any approximation to get the B^0 mass as an signature can never be better as simply to use the $\pi^- X^+$ mass as a signal signature. [3] The expectation for the mass distribution is:

$$M_{\pi X}^2 = M_B^2 + M_D^2 - 2\; E'_B E'_D + 2\; |\vec{p}'_B||\vec{p}'_D| \cos\vartheta' \tag{1.8}$$

[3] If X^+ is a broad resonance, it is better to use the quantity

$$\cos\vartheta' = \frac{M_{\pi X}^2 - M_D^2 + 2.E'_B E'_D - M_B^2}{2.\; |\vec{p}_B||\vec{p}_D|} \tag{1.7}$$

Since the mass is a function of the D^* decay angle, the distribution depends on the D^* polarization which has to been taken into account in the Monte Carlo simulation.

Now let us come to the problem to get the B^0 3-momentum. It can be easily solved in the $\pi^- X^+$ rest frame. In this frame the energy of the B^0 is:

$$E_B^* = \frac{M_B^2 + M_{\pi X}^2 - M_{mis}^2}{2M_{\pi X}} \tag{1.9}$$

The mass M_{mis} of the missing system is simply the D^0 mass. We write the formula in the more general form with an unknown mass M_{mis} for later applications. Due to the small angle between the π_D^- and the D^{*-}, the B^0 momentum is in good approximation parallel to the momentum of the π_D^-:

$$\vec{p}_B^{\,*} \approx \sqrt{(E_B^*)^2 - M_B^2} \cdot \frac{\vec{p}_{\pi_D}^{\,*}}{|\vec{p}_{\pi_D}^{\,*}|} \tag{1.10}$$

For the reconstruction we are using the B^0 momentum from equation 1.10 after a boost in the laboratory frame. The $\pi_D^- X^+$ mass will be the signature for the decay.

1.2.2 The Decay $B^- \to X^+ D^{*-} \pi^+$

Table 1.1 shows that the branching ratio of the decay $B^- \to \pi^- \pi^- D^{*+}$ is of the same order as for the decay $B^0 \to \pi^+ D^{*-}$. Decays of the type $B^- \to X^+ D^{*-} \pi^+$ can therefore result in an substantial background for the B^0 reconstruction.

The reconstruction method explained above for a B^0 can be applied for B^- decays just by replacing X by $X\pi_{D^{**}}$ in the formulas above. Reconstructing B^- mesons can help to reduce background in the B^0 sample.

1.3 Application for the decays $B^0 \to \pi^+ D^{*-}$ and $B^0 \to \rho^+ D^{*-}$

From table 1.1 follows that the decays $B^0 \to (\pi, \pi\pi, \pi\pi\pi) D^{*-}$ are dominated by two body decays. Most important for this analysis are the decays $B^0 \to \pi^+ D^{*-}$ and $B^0 \to \rho^+ D^{*-}$.

1.3.1 The decay $B^0 \to \pi^+ D^{*-}$

For this decay the previous formulas hold replacing X^+ by π^+. In this case the B^0 direction can be approximated using relation 1.10 with $M_{mis} = M_D^0$. The signature of the decay is the $\pi_B^+ \pi_D^-$ mass. Figure 1.1 shows the expected mass distribution. The structure of the mass distribution reflects the polarization of the D^{*-} in this decay which results in an angular distribution:

$$\frac{dN}{d\ \cos\vartheta^*} \propto \cos^2\vartheta^* \tag{1.11}$$

as a signature because E_B' is no longer constant.

where ϑ^* is the D^{*-} decay angle. The relation between the $\pi_B^+\pi_D^-$ mass and this angle is given by equation 1.8.

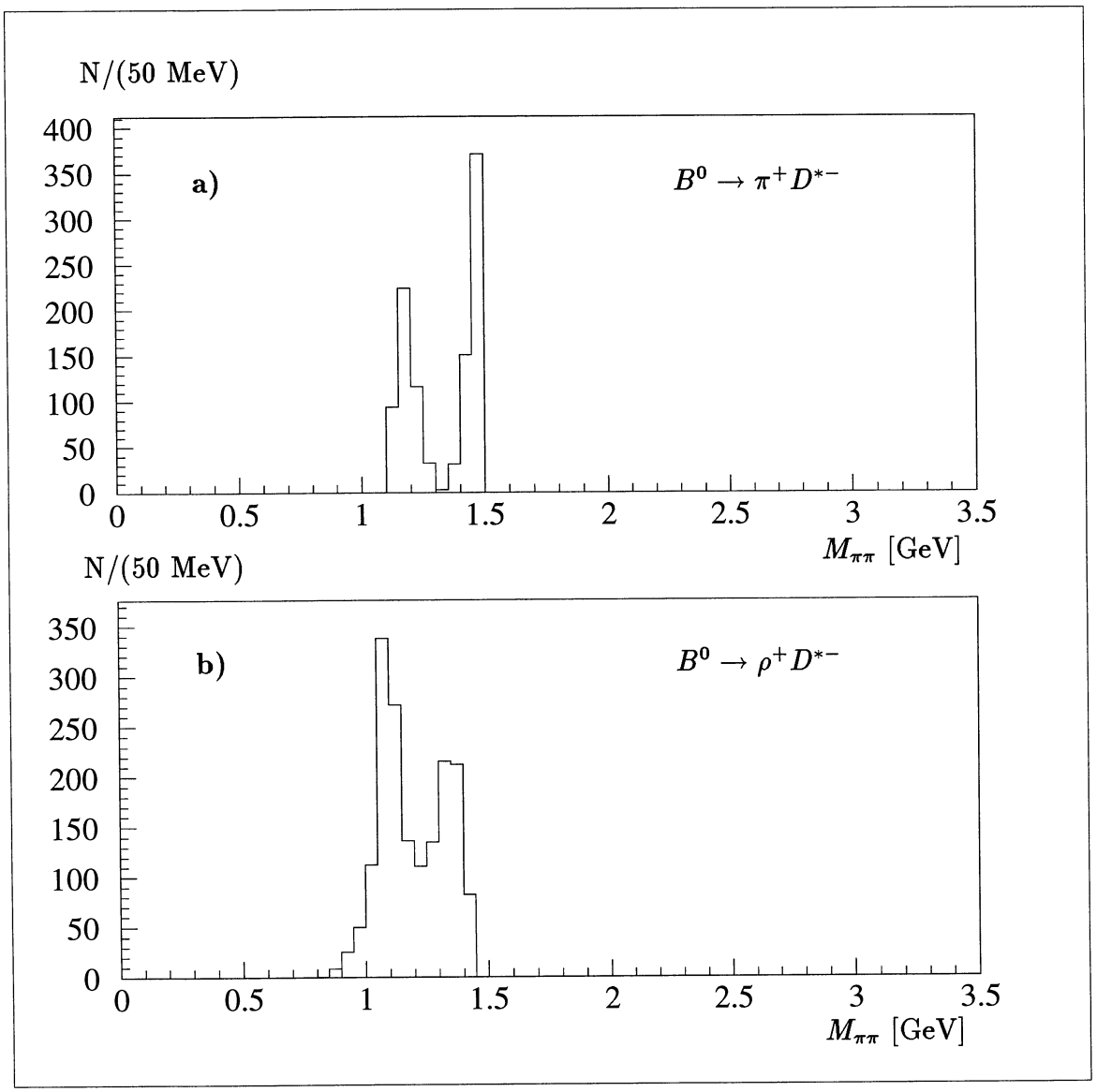

Figure 1.1: Invariant mass of the reconstructed charged pions for a simulation of the decays $B^0 \to \pi^+ D^{*-}$ and $B^0 \to \rho^+ D^{*-}$. Both decays were simulated with longitudinal polarization.

1.3.2 The decay $B^0 \to \rho^+ D^{*-}$

This decay can be handled in the same way as the decay $B^0 \to \pi^+ D^{*-}$. However the longitudinal polarization (see table 1.1) of the ρ^+ allows a reconstruction of

$B^0 \to \rho^+ D^{*-}$ without detecting the π^0 coming from the ρ^+ decay.

In the B rest frame a longitudinal polarization of the ρ^+ means that the angles between the ρ^+ and the pions from the ρ^+ decay is small. Either the neutral or the charged pion is carrying most of the ρ^+ momentum. In half of the decays the neutral pion is slow and the $\pi^0 D^0$ mass in the decay is close to the D^0 mass. These are the decays where a reconstruction of the π^0 is not necessary. The missing mass $M_{\pi^0 D^0}$ is shown in figure 1.2. To get the B momentum an averaged value for the missing mass has to been used in equation 1.10. This still gives a good approximation for the B energy since the right side of formula 1.9 is dominated by the term $M_B^2/2M_{\pi\pi}$. Also the assumption that the direction of the B^0 is parallel to the direction of the soft pion π_D is still a good approximation.

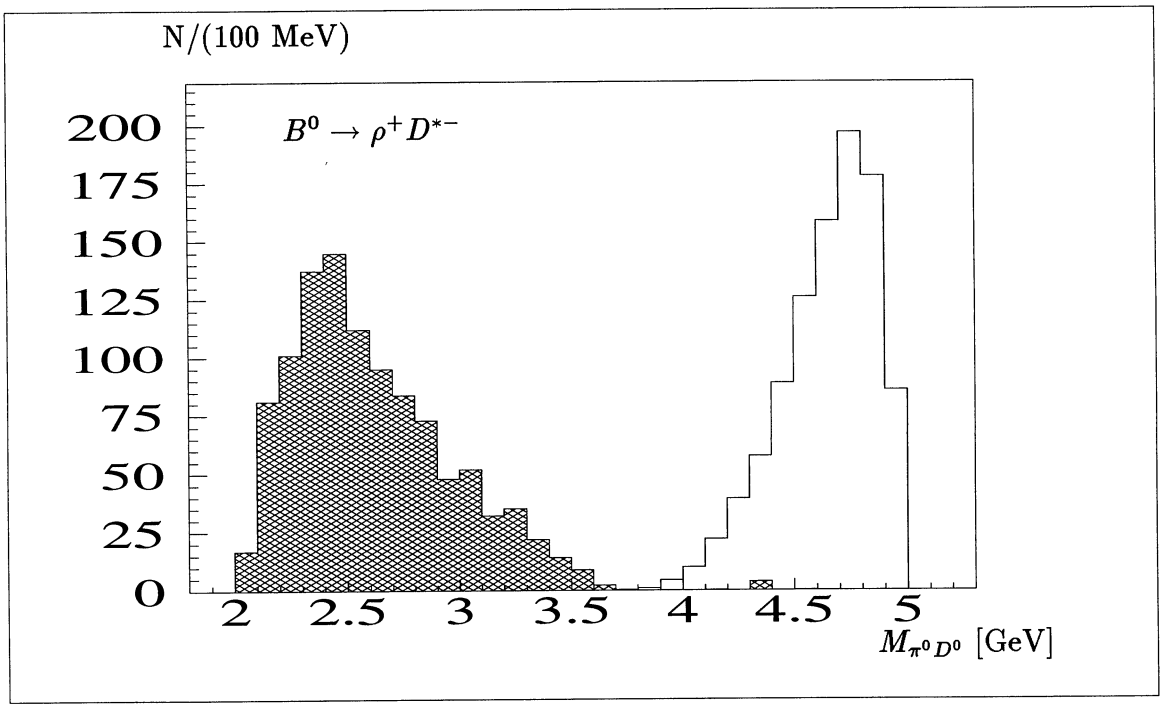

Figure 1.2: Invariant $\pi^0 D^0$ mass for the decay $B^0 \to \rho^+ D^{*-}$. The shaded histogram shows the contribution for $\cos\vartheta_{\rho^+,\pi^+} > 0$. The two maxima in the distribution are due to the longitudinal polarization.

Therefore a reconstruction is possible using again only two charged pions and replacing M_{mis} in equation 1.9 by an averaged missing mass. The signature again is the $\pi^+\pi^-$ mass.

1.3.3 The decay $B^0 \to a_1^+ D^{*-}$

On the first sight this decay mode seems to be similar to $B^0 \to \rho^+ D^{*-}$. Also for $B^0 \to a_1^+ D^{*-}$ a polarization of the a_1^+ is expected. But due to the dominance of

the S-wave in the decay $a_1 \rightarrow \rho\pi$ a reconstruction is only possible if the a_1^+ is fully reconstructed. This leads to a large combinatorial background and disfavors to use this decay mode.

1.3.4 A mixture of the decays $B^0 \rightarrow \pi^+ D^{*-}$, $B^0 \rightarrow \rho^+ D^{*-}$

As explained these decays can be identified by the reconstruction of two charged pions. The kinematics of the two decays are so similar that a separation is not possible. Therefore both decays has to be studied together. First, on has to decide which mass M_{mis} to use in formula 1.9. For a decay $B^0 \rightarrow \pi^+ D^{*-}$ this mass is the D^0 mass. In the case of $B^0 \rightarrow \rho^+ D^{*-}$ the distribution of the missing mass has already been shown (figure 1.2). For a mixture of both decays an averaged value must be determined by Monte Carlo studies. The most important quantity for the background suppression is the direction of the B^0. Therefore the value for M_{mis} was chosen in such a way that the angular resolution of the reconstructed B^0 direction is minimal. A value of $M_{mis} = 2.1$GeV gives the best resolution (see figure 1.3).

The next section will describe the B^0 reconstruction in the data. The aim of the selection is to select decays of the type $B^0 \rightarrow \pi^+ D^{*-}$ and $B^0 \rightarrow \rho^+ D^{*-}$ which will give the best B momentum resolution. As will be seen later, 63 % of the B^0, found in the data, are coming from the decays $B^0 \rightarrow \pi^+ D^{*-}$ and $B^0 \rightarrow \rho^+ D^{*-}$.

1.4 Reconstruction of hadronic B^0 decays

The method will now be used to reconstructed B^0 decays in the ALEPH data. The main background suppression is obtained by the constraint that the reconstructed pions are coming from a secondary vertex and from the fact that the B^0 direction determined from the $\pi_B^+ \pi_D^-$ system has to agree with the B^0 direction obtained from the jet direction and vertex information. Before describing the data selection the determination of the B^0 direction form the jet and vertex information will be explained.

1.4.1 The B^0 flight direction

The best estimation for the B^0 direction of flight can be obtained by combining the information from the jet direction and the vertex information. Jets are built using the JADE-Cluster algorithm with a value of 0.008 for the parameter YCUT. At smaller values for YCUT tails in the resolution function appear (see figure 1.4). The studies on the resolution are based on Monte Carlo events with a mixture of $B^0 \rightarrow \pi^+ D^{*-}$ and $B^0 \rightarrow \rho^+ D^{*-}$.

A parametrization of the angular resolution will be used to combine the jet direction with the vertex information. The following ansatz was chosen for this parametrization:

$$\sigma_\beta(E_B/E_{jet},\ \cos\vartheta_{jet}) = \sigma_\phi(E_B/E_{jet}) \cdot f(\cos\vartheta_{jet}) \tag{1.12}$$

E_B is the B^0 energy as determined from the $\pi_B^+ \pi_D^-$ system and ϑ_{jet} the angle between the jet and the beam axis. The angle β is a projection of the angle between the

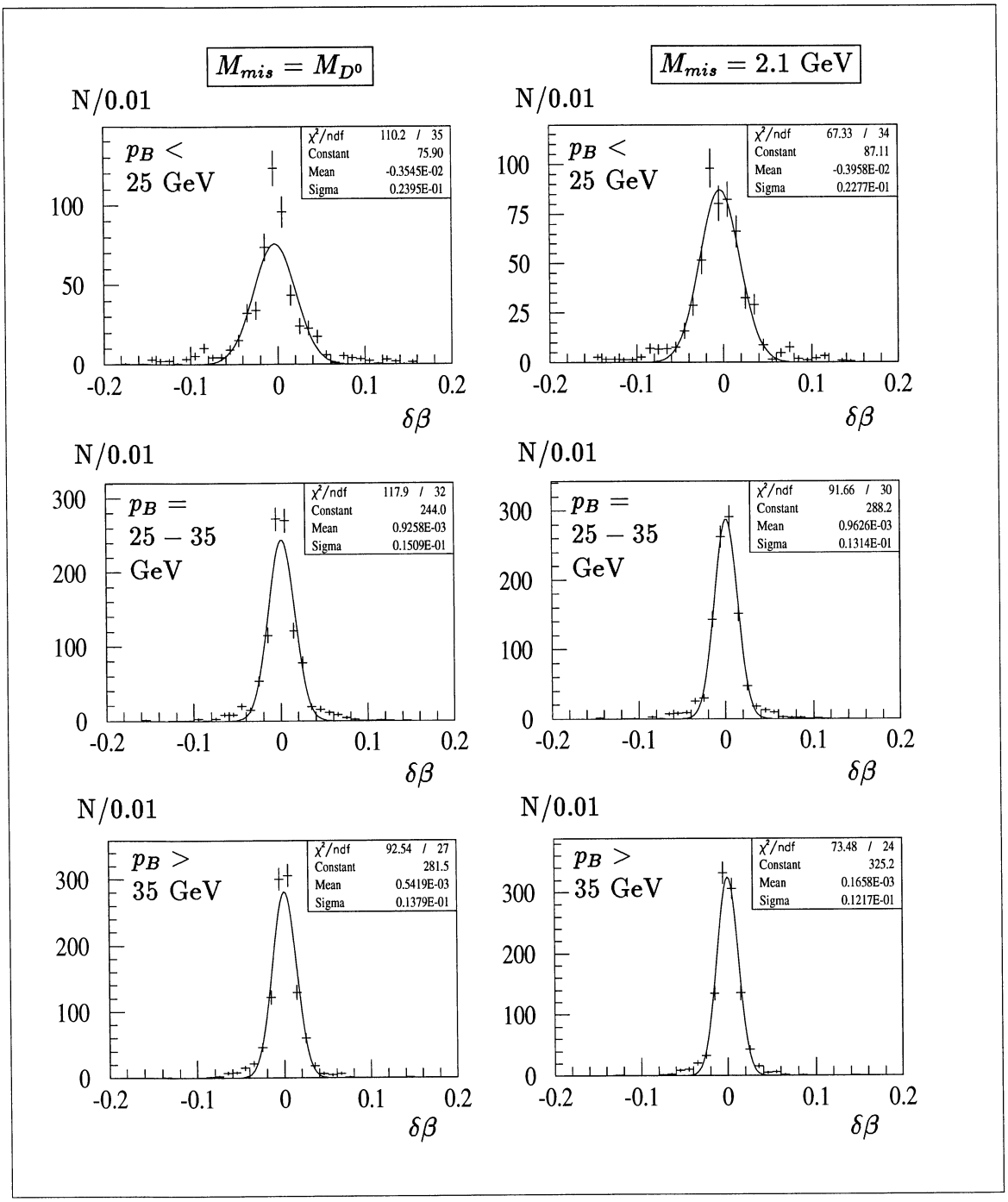

Figure 1.3: Angle between the reconstructed and true B^0 momentum direction for different momentum intervals. The simulation uses a mixture of $B^0 \to \pi^+ D^{*-}$ and $B^0 \to \rho^+ D^{*-}$ events. On the left side the missing mass for the momentum reconstruction was set to $M_{mis} \equiv M_{D^0}$ while on the right side it is $M_{mis} \equiv 2.1$ GeV.

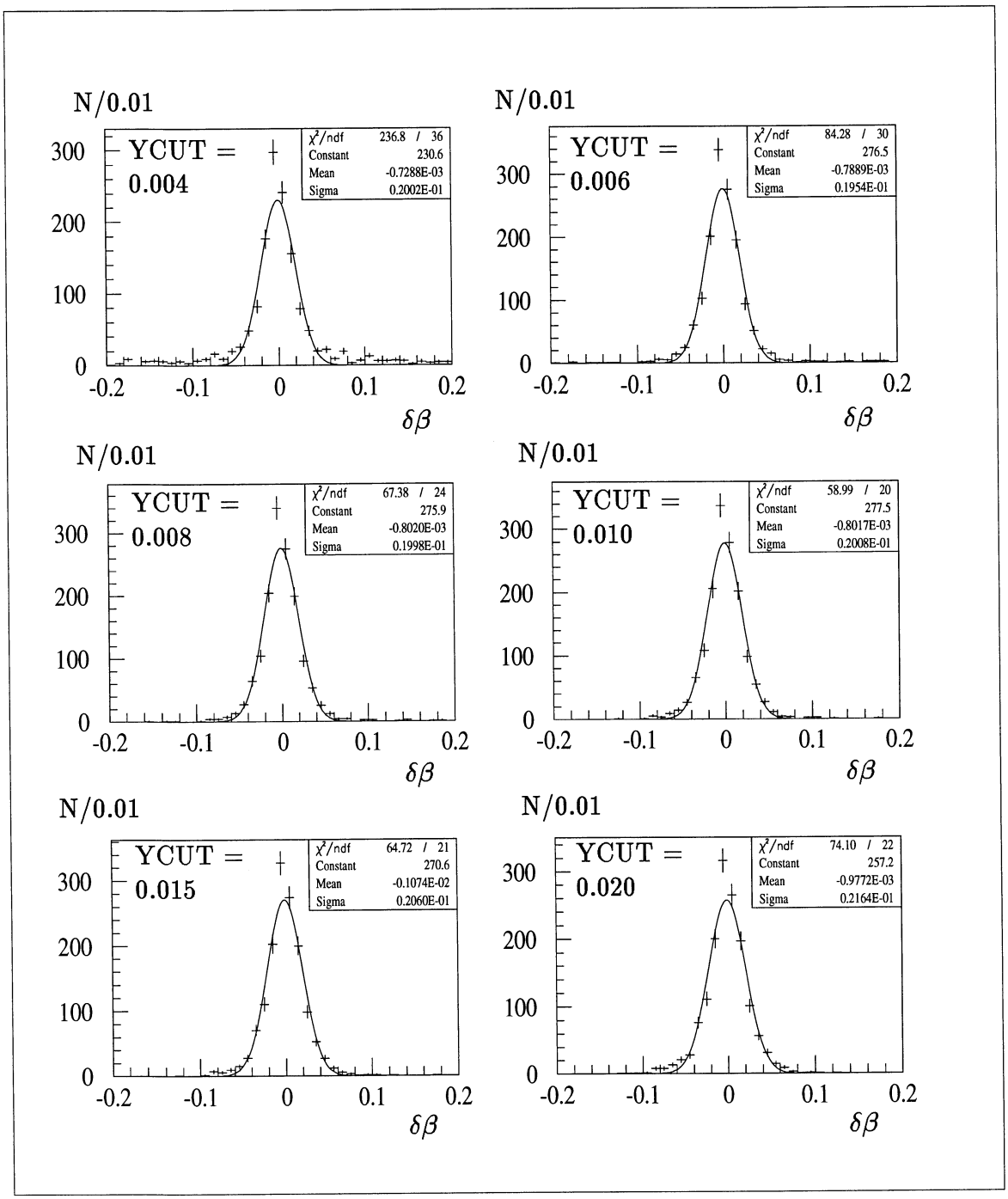

Figure 1.4: Angle between the true B^0 momentum and the jet direction for different values of YCUT in Monte Carlo events.

true B^0 momentum and the jet direction on a plane. The results of a Monte Carlo simulation, displayed in figure 1.5, lead to

$$\sigma_\phi(E_B/E_{jet}) = \left(0.039 - 0.029\frac{E_B}{E_{jet}}\right) \text{ mrad} \quad (1.13)$$

$$f(\vartheta_{jet}) = 0.88 + 0.35\ |\cos\vartheta_{jet}| \quad (1.14)$$

The measurement of the $\pi_B^+\pi_D^-$ vertex is directly a measurement of the B^0 decay vertex. Together with the main vertex the B^0 flight direction is obtained[4].

To combine both informations a χ^2 was minimized to get the vector $\vec{\ell}_B$ between the B^0 production and decay point and the B^0 decay point $\vec{r}_B$. The χ^2 is defined as

$$\chi^2_{dir} = \left(\vec{r}_{main} - \vec{r}_B + \vec{\ell}_B\right)^T V^{-1}_{main}\left(\vec{r}_{main} - \vec{r}_B + \vec{\ell}_B\right) \quad (1.15)$$

$$+ \left(\vec{r}_{\pi\pi} - \vec{r}_B\right)^T V^{-1}_{\pi\pi}\left(\vec{r}_{\pi\pi} - \vec{r}_B\right) \quad (1.16)$$

$$+ \left(\vec{d}_{jet} - \vec{\ell}_B\right)^T V^{-1}_{jet}\left(\vec{d}_{jet} - \vec{\ell}_B\right) \quad (1.17)$$

The matrices V are the covariance matrices for the main vertex$\vec{r}_{main}$, the $\pi_B\pi_D$ vertex $\vec{r}_{\pi\pi}$ and the jet direction $\vec{d}_{jet}$. The minimization leads to set of linear equations to be solved[5]. The improvement in angular resolution is about 10% (see figure 1.6). The error matrix obtained in the minimization procedure includes the uncertainty from the jet direction and the vertex measurements.

The vector $\vec{\ell}_B$ together with the B^0 momentum approximation allows to get the lifetime:

$$t = \frac{\ell_B \cdot M_B}{p_B \cdot c} \quad (1.20)$$

1.4.2 Data Selection

For this study data from '91, '92 and '93 were used. The selection starts with the reconstruction of pions.

- **The $\pi_B^+\pi_D^-$ selection:**
  any track is defined as $\pi^\pm$ candidate if not identified as lepton or belonging to a V0 (KEFOTY = 0). In addition an existing dE/dx measurement with more than 50 measured points has to agree with the pion hypothesis within 3 standard deviations.

[4]The main vertex was determined using the QFNDIP routine.

[5]The vector $\vec{r}_B$ is used later to look for additional pions coming from the B vertex. If only $\vec{\ell}_B$ is needed the χ^2 is simpler:

$$\chi^2_{dir} = \left(\vec{r}_{\pi\pi} - \vec{r}_{main} - \vec{\ell}_B\right)^T V^{-1}_{\pi\pi,main}\left(\vec{r}_{\pi\pi} - \vec{r}_{main} - \vec{\ell}_B\right) \quad (1.18)$$

$$+ \left(\vec{d}_{jet} - \vec{\ell}_B\right)^T V^{-1}_{jet}\left(\vec{d}_{jet} - \vec{\ell}_B\right) \quad (1.19)$$

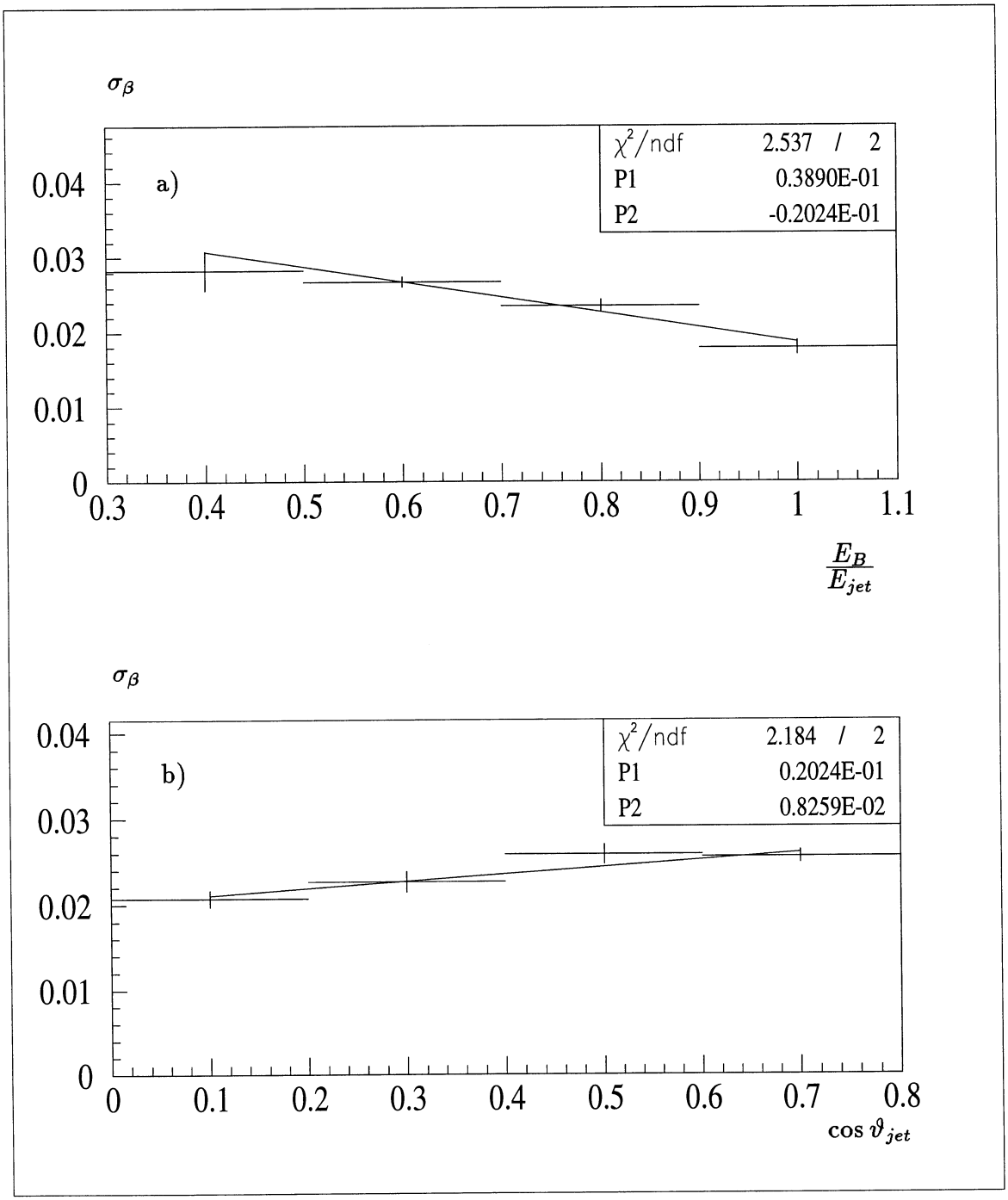

Figure 1.5: Angular resolution of the B^0 direction determined from the jet axis and the vertex information. The dependence on the ratio E_B/E_{jet} is shown in figure **a)**. In figure **b)** the resolution is given as a function of the jet direction.

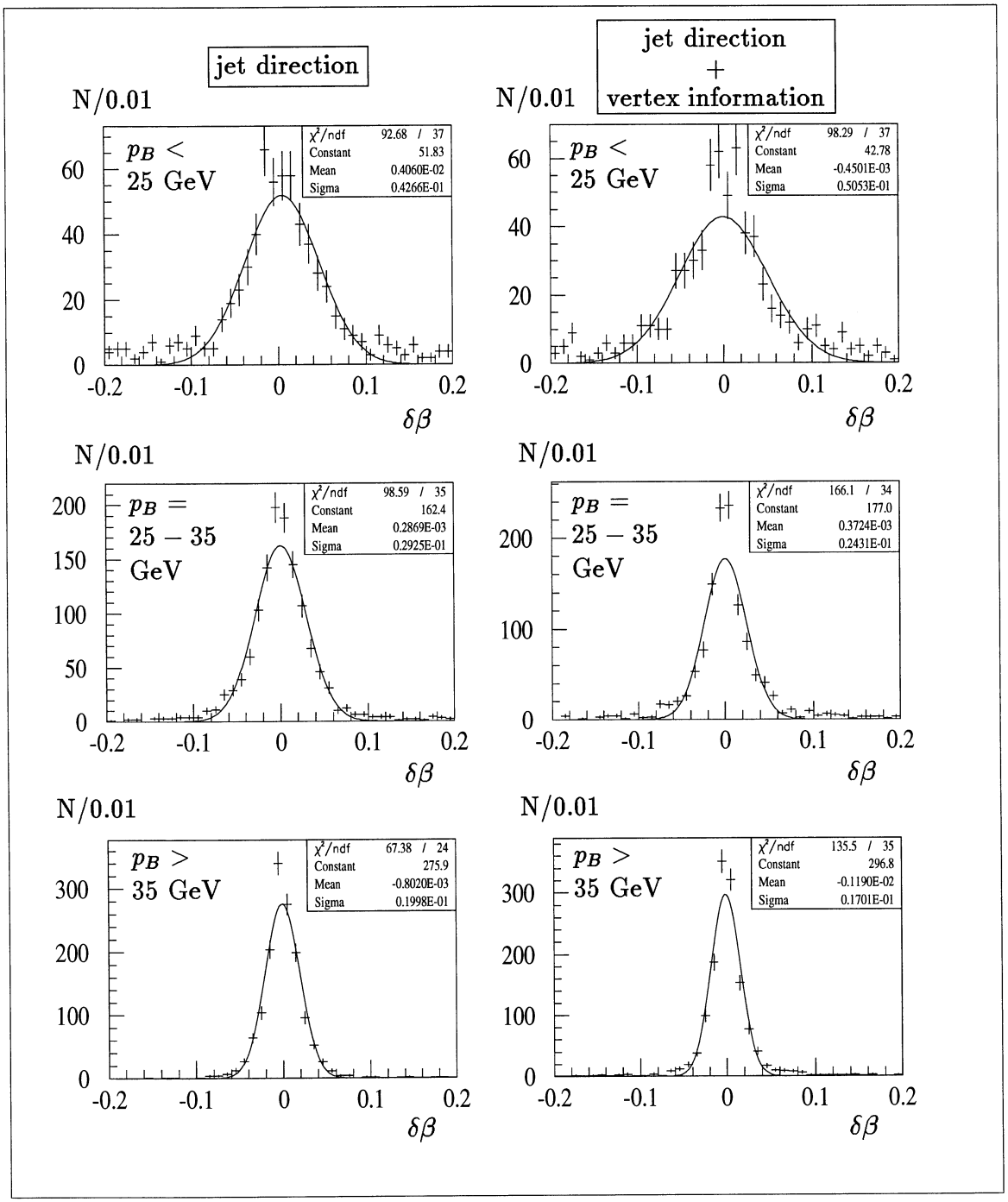

Figure 1.6: Angle between the true B^0 momentum and the reconstruction of the B^0 direction using the jet direction (on the left). On the right sight the vertex information is included.

Two charged pions $\pi_B^+\pi_D^-$ are selected. A vertex fit is applied to get the B^0 decay vertex (YTOPOL). Pion combinations are accepted if $\chi^2_{\mathrm{YTOPOL}}/NoF < 9$.

- **B^0 flight direction:**
The B^0 flight direction was obtained by using the jet which contains the fast pion π_B^+. The jet was required to lie in the central part of the detector:

$$|\cos\vartheta_{jet}| < 0.7 \tag{1.21}$$
$$\tag{1.22}$$

The jet direction has to agree with the B^0 with the B^0 flight direction from the vertices

$$\chi^2_{dir} < 4 \tag{1.23}$$

See equation 1.17 for the definition of χ^2_{dir}.

- **B^0 lifetime :**
In this study candidates with a proper time

$$20 \text{ ps} > t > 1 \text{ ps} \tag{1.24}$$

were used. The cut at 1 *ps* was made to suppress background from u, d, s and c events.

- **B^0 kinematics:**
The approximation of the B^0 momentum was determined following the technique described above. $\pi_B^+\pi_D^-$ candidates fulfilling

$$30 \text{ GeV} < |\vec{p}_B| < 45 \text{ GeV} \tag{1.25}$$
$$|\cos\vartheta^*_{B,\pi_B^+}| < 0.8 \tag{1.26}$$

are accepted (see figure 1.7). The requirement on the B^0 decay angle ϑ_{B,π_B^+} is similar to a p_t cut but does not effect the $\pi^+\pi^-$ mass distribution.

- **Comparison of B^0 flight direction:**
The angle α between the B^0 flight direction $\vec{\ell}_B$ from the jet/vertices and the approximation of the B^0 momentum $\vec{p}_B$ is displayed in figure 1.8 for a simulation of the signal and the data. A cut at

$$\alpha < 0.025 \tag{1.27}$$

was chosen.

- **$B^+ \to \pi^+ X D^{**0}$ suppression:**
Applying the cuts above the expected background from B^+ decays is $N(B^+ \to D^{*-})/N(B^{+,0} \to D^{*-}) = 0.17$ according to a Monte Carlo simulation. To reduce the B^+ background it was searched for candidates for the B^+ decay

$$B^+ \to \pi^+\pi^+ X D^{*-} \tag{1.28}$$

For a candidate the additional π^+ must be found:

- dEdx: $\chi^2_\pi < 4$, $\chi^2_K > 1$.
- the pion comes from the B vertex:

$$prob^{impactparameter}_{main\ vertex} < 5\% \quad (1.29)$$
$$prob^{impactparameter}_{\pi\pi\ vertex} > 5\% \quad (1.30)$$

- The B^+ flight direction can be calculated in the same way as for a B^0 candidate using $M_{mis} = M_{D^0}$ in formula 1.9. The measured hadronic system X are the two charged pions $\pi^+\pi^+$. The angle α was required to be smaller than $\alpha < 0.02$.

This selection has an efficiency of 60 % for $B^+ \to pi^+\pi^+ X D^{*-}$ events. Due to the rejection of these events only 20% of the B^0 decays are lost.

The $\pi^+\pi^-$ mass distribution for all combinations which pass the cuts is given in figure 1.9. It shows an enhancement at small masses. This distribution has to be compared with the expected background and the expected signal.

1.4.3 Background

In figure 1.9 the data spectrum is compared with the Monte Carlo simulation. The Monte Carlo spectrum consists of two contributions:

- D^* events where the two pions are coming from a $B^0 \to \pi^-_B X D^{*-} \to \pi^-_B X \pi^-_D D^0$ or $B^+ \to \pi^-_B X D^{*-} \to \pi^-_B X \pi^-_D D^0$ or decay. Kinematics restricts the $\pi^+\pi^-$ mass to the region below 1.5 GeV.

- Background events are all remaining events from $q\bar{q} = u\bar{u}, d\bar{d}, s\bar{s}, c\bar{c}$ and from $b\bar{b}$ production. The $q\bar{q}$ background is shown as hatched histogram in figure 1.9. The dashed histogram shows the sum of both contributions. The background is normalized using the region above 1.5 GeV. The numbers of expected events in the signal region are listed in table 1.2. A normalization using the luminosities yields 56.5 instead of 49.3 background events. The scaling error includes a systematic uncertainty of 7.5% (see section 2.1.3).

The number of expected signal events is in agreement with the observed number of events. For the simulation of the signal events see appendix A.

The ratio of $B^+/(B^0 + B^+)$ events in the D^* events is $8.9 \pm^{2.9}_{3.0}$ % in the Monte Carlo. Two other methods were used to estimate this ratio. A fit was done to the background subtracted spectrum (figure1.9) with free B^0 and B^+ contributions. This gives $B^+/(B^0 + B^+) = 0.00 \pm^{0.10}_{0.00}$. The second method is using the selected B^+ candidates with three pions, which were rejected in the analysis. The $\pi^+\pi^-$ mass spectrum for these events is given in figure 1.10. The Monte Carlo clearly shows the enhancement of the B^+ contribution in this sample. Assuming that the relative rates $\#B^0_{\pi\pi}/\#B^0_{\pi\pi\pi}$ and $\#B^+_{\pi\pi}/\#B^+_{\pi\pi\pi}$ from the Monte Carlo are predicted correctly, the absolute numbers can be obtained by using the background subtracted data. This

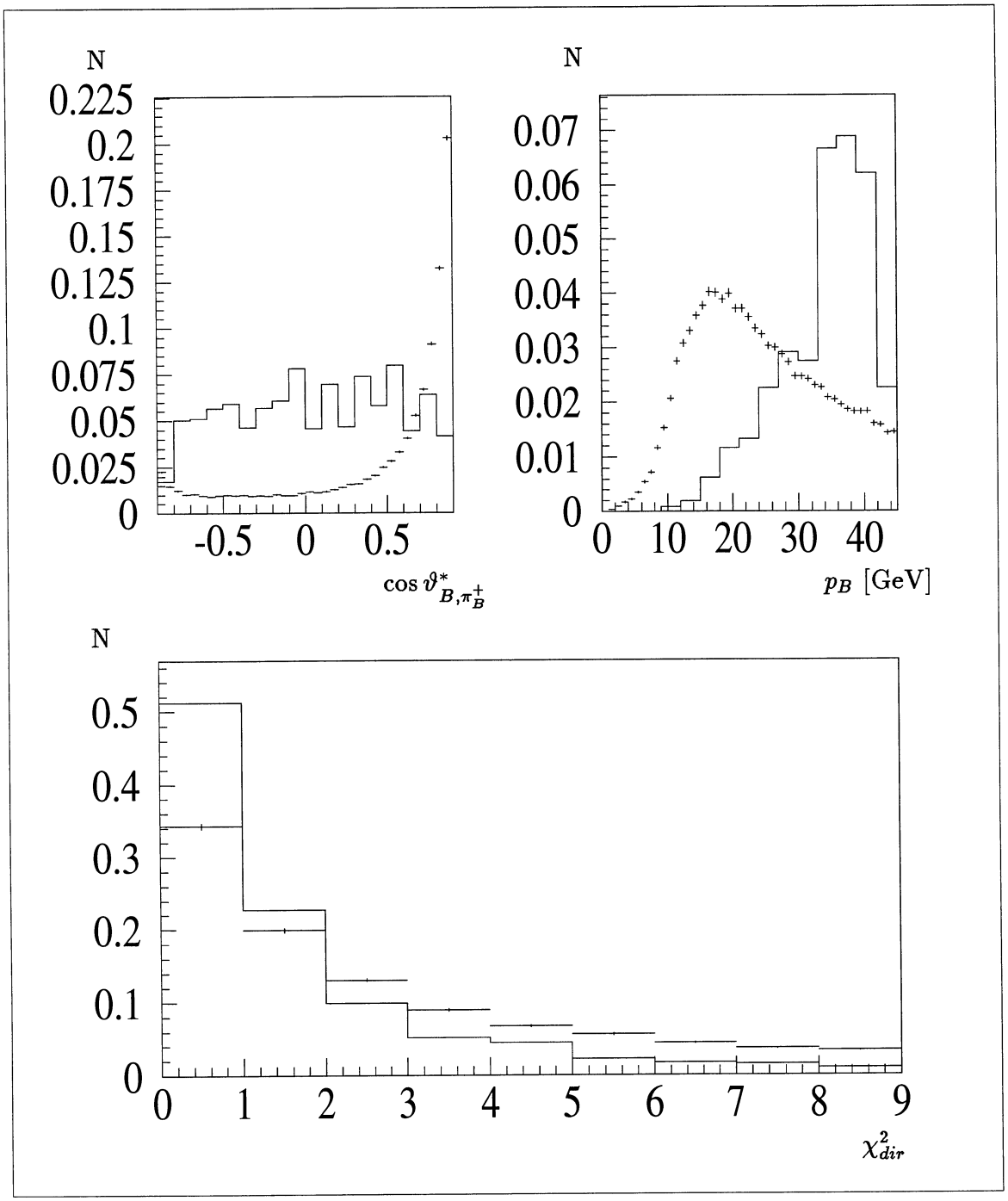

Figure 1.7: $\cos\vartheta^*_{B,\pi^+_B}$, p_B and χ^2_{dir} distributions for data (crosses) and Monte Carlo $B^0 \to \pi^+, \rho^+ D^{*-}$ events (histogram).

leads to a ratio of $B^+/(B^0 + B^+) = 0.00 \pm 0.07$. Both results are in agreement with the Monte Carlo expectation of $B^+/(B^0 + B^+) = 8.9 \pm^{2.9}_{3.0}$ %. To be conservative an

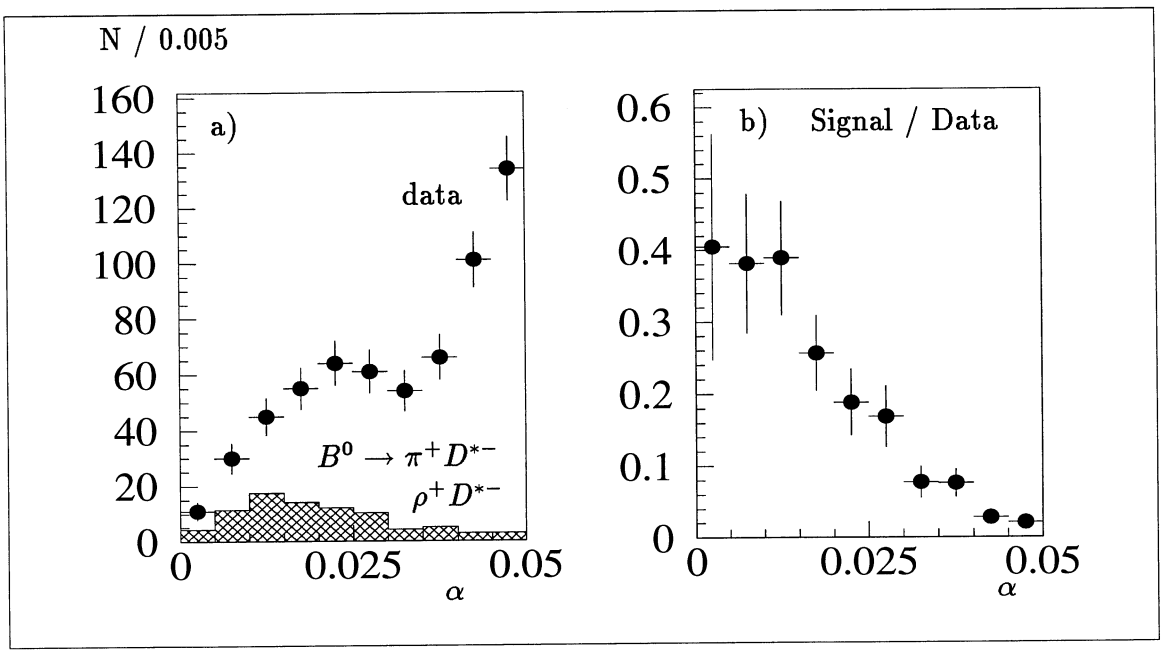

Figure 1.8: χ_α distribution for background and $B^0 \to \pi^+, \rho^+ D^{*-}$ simulations (figure **a)**) in the mass region $M_{\pi\pi} = 1. - 1.5$ GeV. Figure **b)** displays the expected ratio of signal to background.

additional error of 50% was added:

$$\frac{B^+}{B^0 + B^+} = 8.9 \pm^{2.9}_{3.0} \pm 4.5\% \tag{1.31}$$

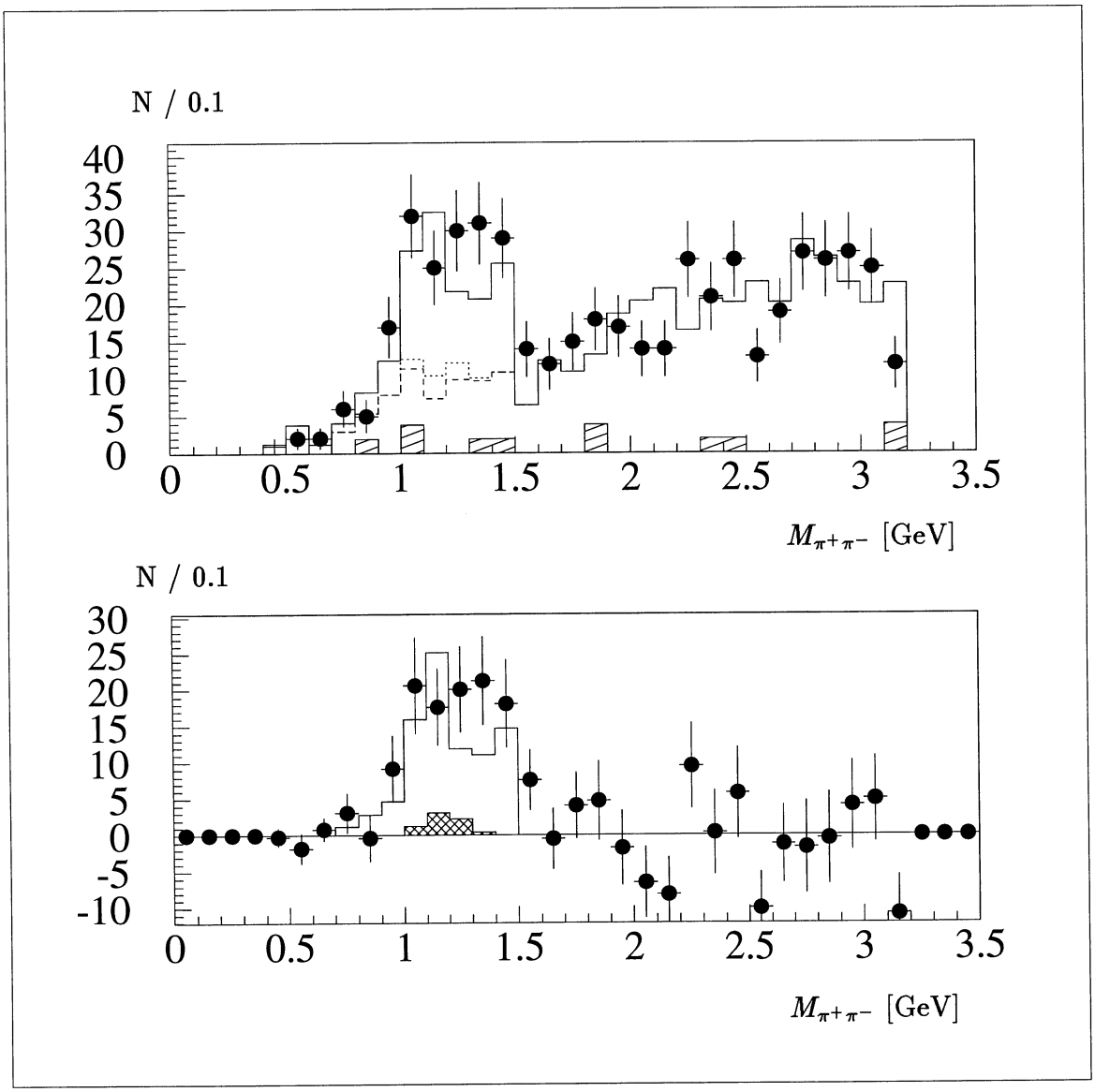

Figure 1.9: $\pi_B^+\pi_D^-$ mass distributions. Shown are in figure **a)** the data (with error bars) and the Monte Carlo simulation (histograms). In the histograms the contributions from $q\bar{q}$ background, $b\bar{b}$ background, $B^+ \to \pi_B^+ X D^{*-}$ and the $B^0 \to \pi_B^+ X D^{*-}$ signal are added. The dots with error bars in figure **b)** are the data after subtraction of the $q\bar{q}$ and $b\bar{b}$ background. The histograms are the predictions for $B^+ \to \pi_B^+ X D^{*-}$ and the sum of $B^0, B^+ \to \pi_B^+ X D^{*-}$ decays.

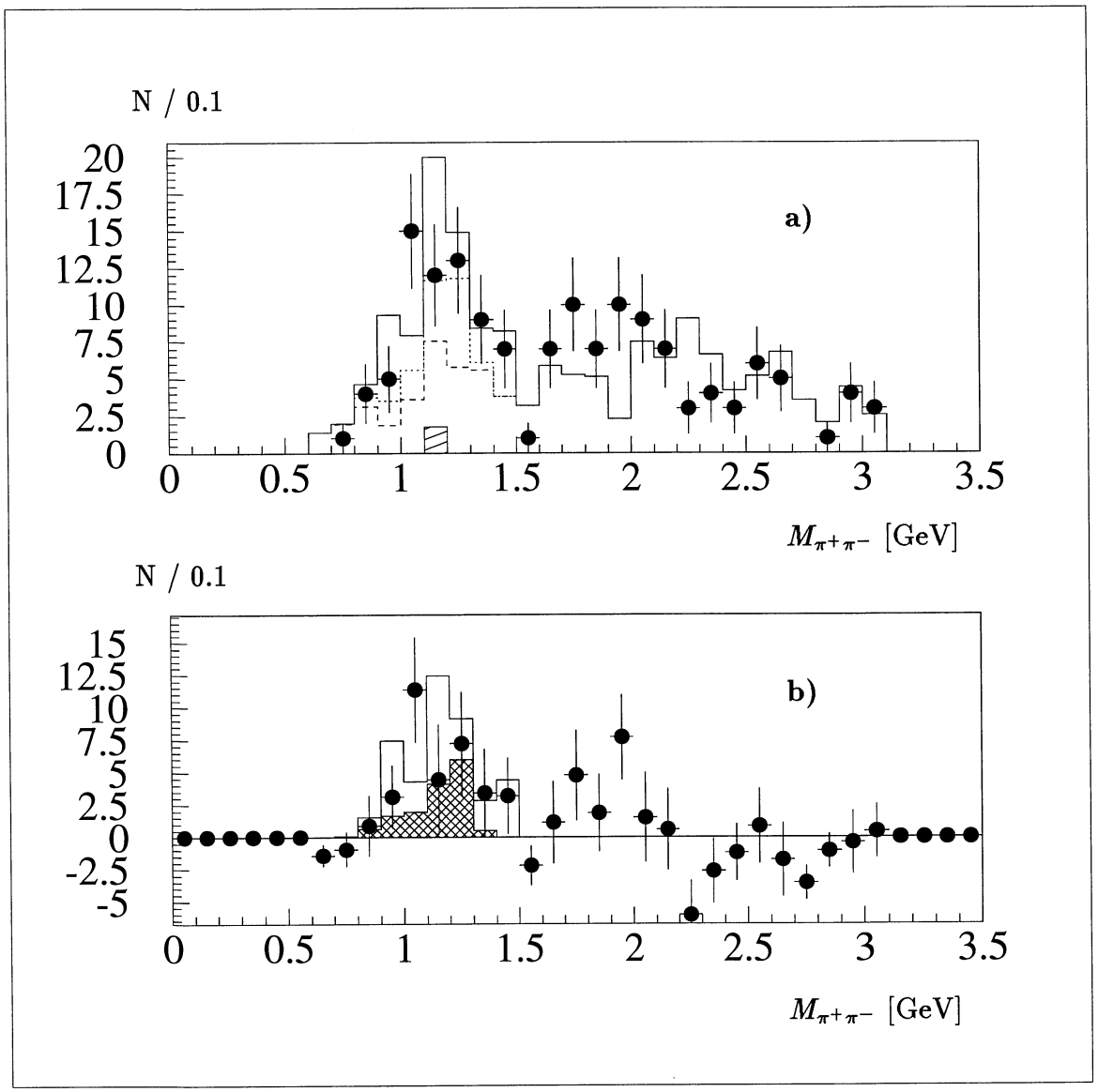

Figure 1.10: $\pi_B^+\pi_D^-$ mass distributions for the B^+ candidates. Shown are in figure **a)** the data (with error bars) and the Monte Carlo simulation (histograms). In the histograms the contributions from $q\bar{q}$ background, $b\bar{b}$ background, $B^+ \to \pi_B^+ X D^{*-}$ and the $B^0 \to \pi_B^+ X D^{*-}$ signal are added. The dots with error bars in figure **b)** are the data after subtraction of the $q\bar{q}$ and $b\bar{b}$ background. The histograms are the predictions for $B^+ \to \pi_B^+ X D^{*-}$ and the sum of $B^0, B^+ \to \pi_B^+ X D^{*-}$ decays.

	# events	systematic errors $\epsilon_b = (32 \pm 17) \cdot 10^{-3}$	systematic errors scaling	total
data	147 ± 12.1			
$b\bar{b}$ background (MC)	41.6 ± 4.5		± 4.3	
$q\bar{q}$ background (MC)	7.7 ± 3.8		± 0.8	
excess	97.7 ± 13.5	$\pm^{0.3}_{0.0}$	± 5.0	97.7 ± 14.4

MC expectations	# events	systematic errors $\epsilon_b = (32 \pm 17) \cdot 10^{-3}$	systematic errors BR	total
$B^0 \to \pi^+ D^{*-}$	25.8 ± 2.1		± 3.8	
$B^0 \to \rho^+ D^{*-}$	19.7 ± 3.3		± 4.1	
$B^0 \to (\pi^+, \rho^+)(\pi^0 D^{*-})_{D^{**}}$	7.8 ± 1.8		± 2.3	
$B^0 \to X_{rest} D^{*-}$	18.4 ± 3.1			
Sum B^0	71.7 ± 5.3	$\pm^{3.1}_{2.4}$	± 6.0	$71.7 \pm^{8.6}_{8.4}$
$B^+ \to \pi^+(\pi^+ D^{*-})_{D^{**}}$	5.4 ± 0.9		± 1.6	
$B^+ \to \rho^+(\pi^+ D^{*-})_{D^{**}}$	1.2 ± 0.7		± 0.4	
$B^+ \to X_{rest} D^{*-}$	0.4 ± 0.4			
Sum B^+	7.0 ± 1.1	$\pm^{0.0}_{0.6}$	± 1.6	$7.0 \pm^{1.9}_{2.0}$
Sum B^0, B^+	78.7 ± 5.4	$\pm^{2.5}_{2.4}$	± 6.2	78.7 ± 8.6
Ratio B^+/B (MC)				$(8.9 \pm^{2.9}_{3.0})\%$
Ratio B^+/B (fit to $M_{\pi^+\pi^-}$)				$(0.0 \pm^{0.10}_{0.0})\%$ $< 12.1\%$ (90% CL)
Ratio B^+/B (B^+ selection)				$(0.00 \pm 0.07)\%$ $< 8.9\%$ (90% CL)

Table 1.2: Observed and expected number of events in the signal mass region $M_{\pi\pi} = 1 - 1.5\ GeV$.

Chapter 2

Measurement of the B^0 Lifetime

The B^0 candidates in the signal mass region $M_{\pi\pi} = 1 - 1.5$ GeV, selected in chapter one, were used to determine the B^0 lifetime from an unbinned maximum likelihood fit. For the fit the expected distributions for the proper time

$$t = \frac{\ell_B \cdot M_B}{p_B \cdot c} \tag{2.1}$$

must be known in an analytical form. The form of these functions for signal and background events will be explained in the next section.

2.1 Signal and background time distributions

The sample of candidates consists of three parts:

- **Signal events** $B^0 \to \pi_B^+ \; X \; (D^0\pi_D^-)_{D^*}$.
- **B^+ background** $B^+ \to \pi_B^+ \; X \; (D^0\pi_D^-)_{D^*}$.
- **combinatorial background**

These three contributions will be discussed separately.

2.1.1 The proper time distribution for the signal

The distribution of the measured time t for B^0 decays is obtained by folding an exponetial with the resolution functions $R^\ell(\ell, \ell_t)\; R^p(p, p_t)$ taking into account the efficiency $\epsilon(\ell_t, p_t)$ and integrating over the measured momentum p ($p \in [p_{min}, p_{max}] = [30\ GeV, 40\ GeV]$).

$$f_s(t) = a_s \int_{p_{min}}^{p_{max}} dp \int dp_t \int d\ell_t \; \underbrace{R^\ell(\ell, \ell_t)\; R^p(p, p_t)}_{\text{resolution functions}} \; \underbrace{\epsilon(p_t, \ell_t)}_{\text{efficiency}} \; \underbrace{g(p_t)}_{\text{momentum spectrum}} \; \underbrace{\frac{1}{\tau}\, e^{-t_t/\tau}}_{\text{decay function}} \tag{2.2}$$

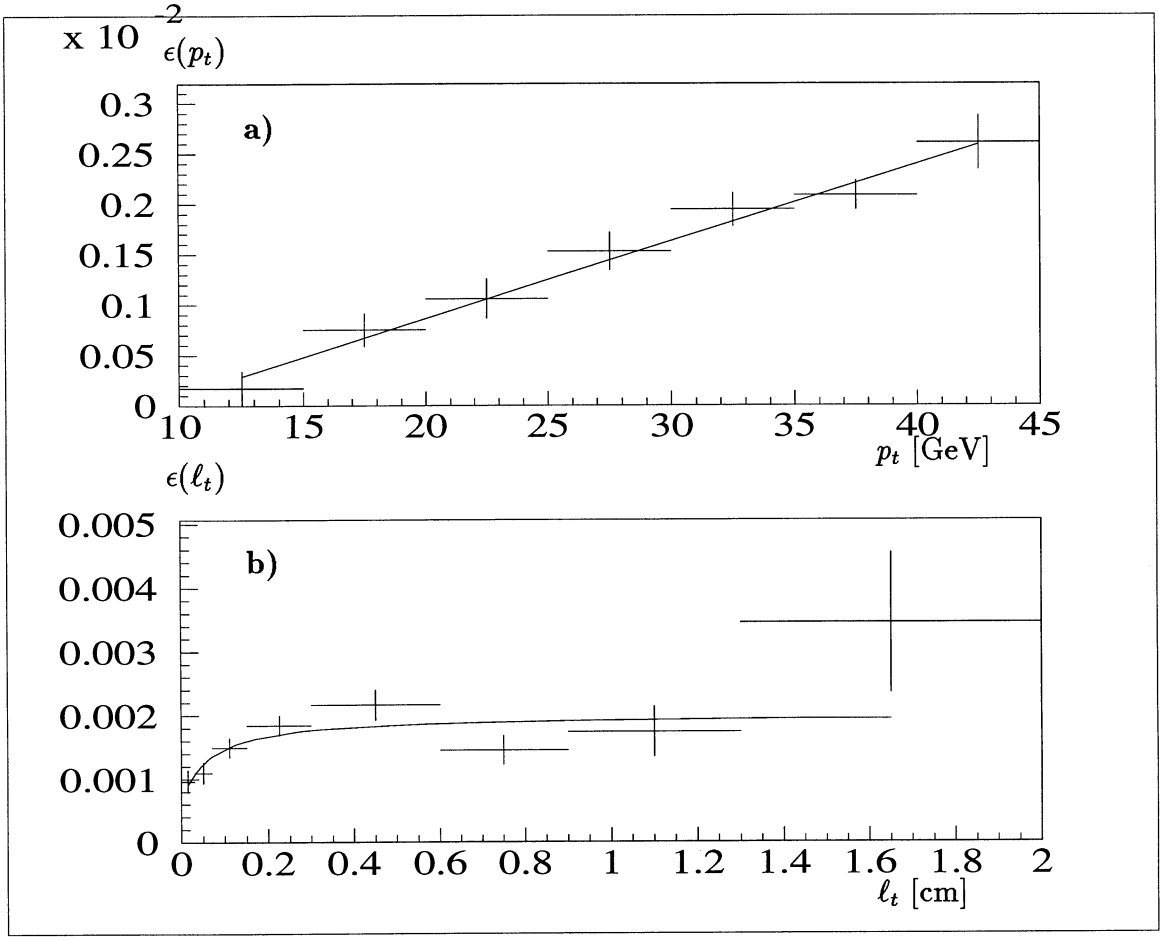

Figure 2.1: Efficiency in Monte Carlo events.

p_t and ℓ_t are the true B^0 momentum and decay length. a_s is a normalization function to guarantee $\int_{t_{min}}^{t_{max}} dt\ f(t) = 1$ for the time region $t \in [t_{min}, t_{max}] = [1\ ps, 20\ ps]$.

The momentum distribution $g(p_t)$ is obtained from Monte Carlo using the measured fragmentation parameter $\epsilon_b = 0.0032 \pm 0.0015$ [27].

The efficiency (figure 2.1) is determined from Monte Carlo events factorizing the p_t and ℓ_t component: $\epsilon(p_t, \ell_t) = \epsilon_p(p_t) \cdot \epsilon_\ell(\ell_t)$.

The decay length and the momentum resolutions are shown in figure 2.2. Parametrizations with two gaussians were used. For completeness the averaged time resolution is shown as well.

For the fit procedure it is convenient to rewrite $f_s(t)$:

$$f_s(t) = a_s \frac{c}{M_B} \int dt_t\ \frac{1}{\tau}\ e^{-t_t/\tau} \underbrace{\int dp_t\ \epsilon(p_t, \ell_t)\ g(p_t) \int_{30\ GeV}^{45\ GeV} dp\ R^\ell(\ell, \ell_t)\ R^p(p, p_t)}\quad (2.3)$$

The time dependent time resolution $G(t, t_t)$ has only to be determined once per fit.

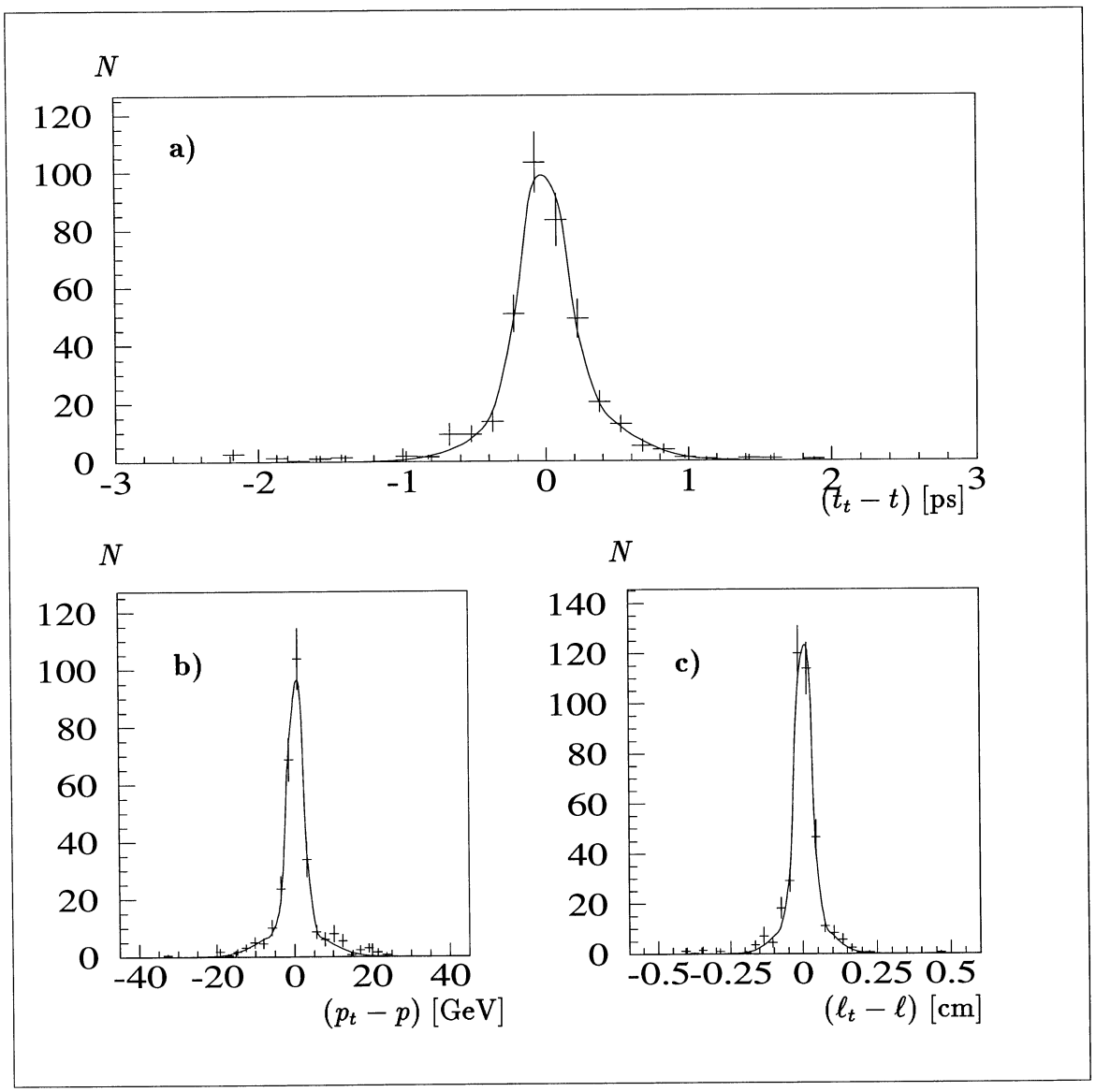

Figure 2.2: Time, momentum and decay length resolution from Monte Carlo events.

2.1.2 The time distribution for $B^+ \rightarrow \pi_B^+ X (D^0\pi_D^-)_{D^*}$ background

This background is the smallest of the three contributions. The corresponding time distribution can be approximated by a simple exponential with an effective B^+ lifetime.

$$f_+(t) = \exp(t, \tau_+) \tag{2.4}$$

$\exp(t,\tau)$ is a normalized exponential:

$$\exp(t,\tau) = \frac{1}{\tau} \cdot \left(e^{-t_{min}/\tau} - e^{-t_{max}/\tau}\right)^{-1} \cdot e^{-t/\tau} \tag{2.5}$$

The effective lifetime $< \tau_+ >= 1.01 \pm 0.17\ ps$ is obtained from Monte Carlo using the world average B^+ lifetime $< \tau_+ >= 1.67 \pm 0.08\ ps$[28].

2.1.3 The time distribution for the combinatorial background

For the combinatorial background a sum of two normalized exponetials was used:

$$f_b(t) = r_b \cdot \exp(t,\tau_{b1}) + (1 - r_b)\exp(t,\tau_{b2}) \tag{2.6}$$

The parameters r_b, τ_{b1} and τ_{b2} are free in the fit but restricted by using data events to describe the background.

One method to describe the background is to use the wrong charge combination, $\pi_B^{\pm}\pi_D^{\pm}$, applying the same selection criteria as for the $\pi_B^+\pi_D^-$ signal candidates. Due to the large difference in the momentum between the two pions (one is assumed to come directly from the B^0 while the second is the slow pion from the D^{*-} decay) the charge correlation is expected to be small for the background. The $\pi_B^{\pm}\pi_D^{\pm}$ mass spectrum for the wrong charge combinations is shown in figure 2.3. A good agreement is found between data and Monte Carlo with no enhancement in the signal mass region.

In addition to the fact that the charge correlation is small, also the correlation between the pion momenta transverse to the jet axis is small for background events. Slow pions are distributed almost symmetric around the jet axis. A second sample was obtained selecting events with $\pi_B^+\pi_D^-$ combinations by first rotating the π_D^- around the jet axis in such a way that the difference in momentum before and after the rotation is 200 MeV. The rotation angle β which can be either positive or negative was restricted to $|\beta| \leq 90°$. This rotation is large enough to destroy the kinematical correlation for signal events. This sample is called $\pi_B^+\ rot(\pi_D^-)$ sample.

A third sample, $\pi_B^{\pm}\ rot(\pi_D^{\pm})$, was selected by using wrong charge combinations together with a rotation around the jet axis.

The $\pi\pi$ mass distributions for the three samples are shown in figure 2.3. The data are well described by the Monte Carlo. For the final fit all three samples were used together.[1] The assumption that the time distribution of the background sample describes the real background can be tested using Monte Carlo and for the $\pi\pi$ mass region $m_{\pi\pi} > 1.5\ GeV$ where no signal events can contribute (see figure 2.4).

The number of expected background events in the signal mass region $m_{\pi\pi} = 1 - 1.5$ GeV was already determined in chapter one by an extrapolation from Monte Carlo events:

$$N_{m=1-1.5}^{expected} = N_{m=1-1.5}^{MC} \frac{N_{m>1.5}^{data}}{N_{m>1.5}^{MC}} \tag{2.7}$$

The correctness of this extrapolation can be checked using the background sample. For the background sample the corresponding estimated number of events is:

$$N_{m=1-1.5}^{expected} = 147.1 \pm 11.0 \tag{2.8}$$

[1] No double entries were found in the samples.

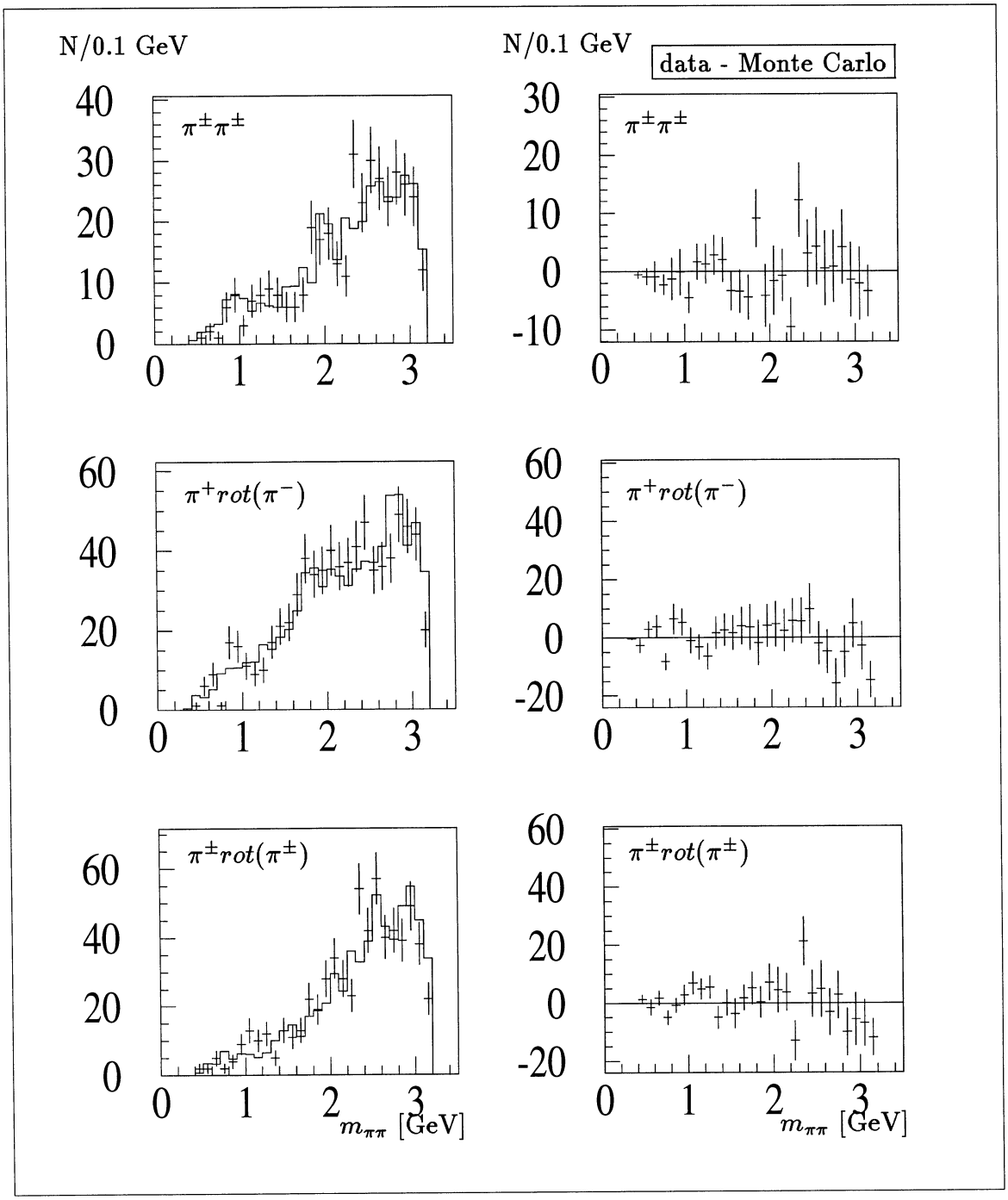

Figure 2.3: Comparison of the $\pi\pi$ mass distribution for data and Monte Carlo background samples.

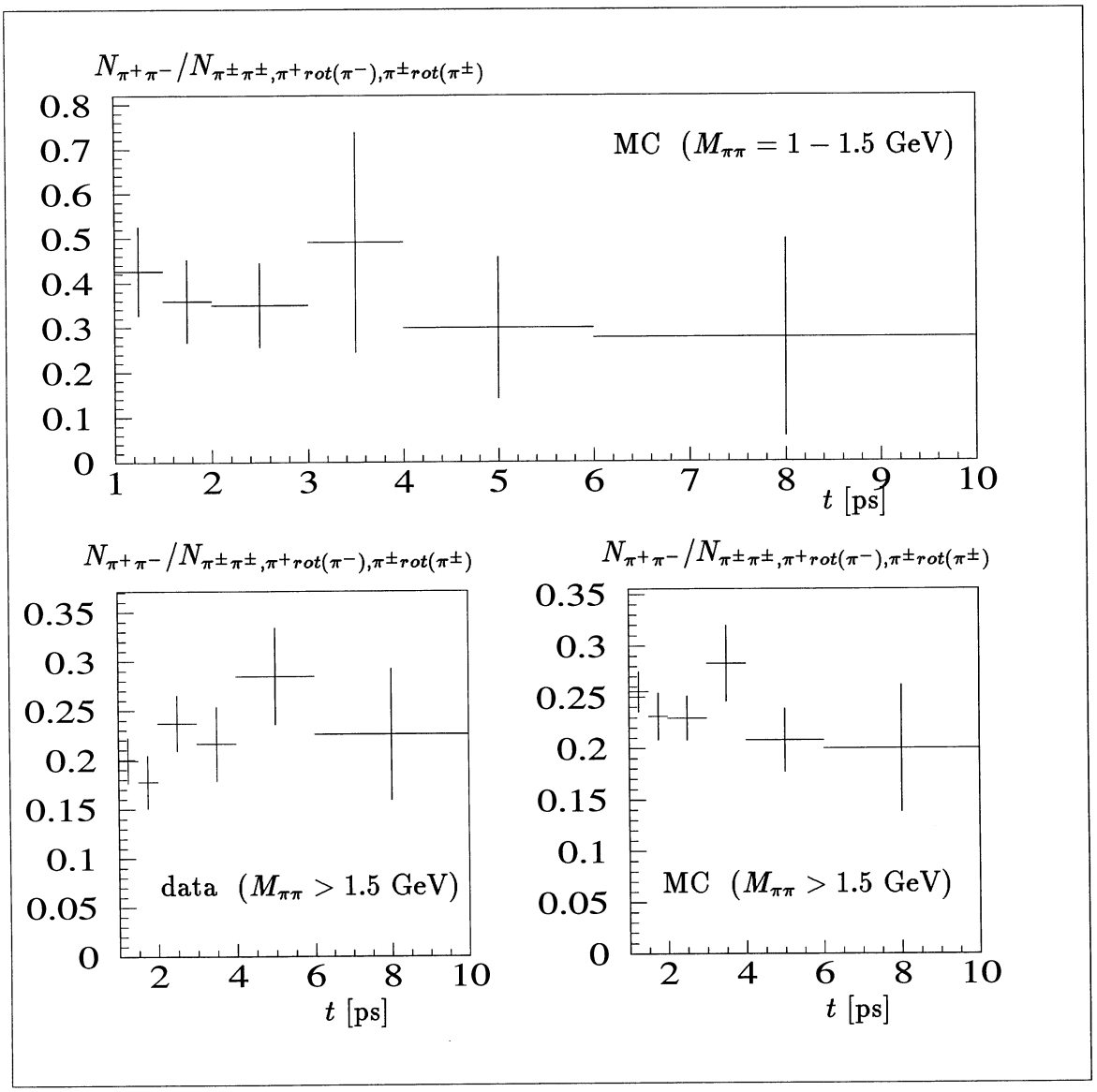

Figure 2.4: Ratio of background events in the $\pi^+\pi^-$ sample and events in the background sample. The upper figure shows the ratio for Monte Carlo events in the signal mass range. In addition the ratio is given in the mass range above 1.5 GeV for Monte Carlo events and data.

to be compared with $N_{1-1.5}^{data} = 156$. The accuracy of this test is $11.0/147.1 = 0.075$ which is taken as the systematic error on the number of expected background events in the signal sample.

2.2 The lifetime fit

The B^0 lifetime was obtained from an unbinned maximum likelihood fit. The fit parameters are:

τ_0	: B^0 lifetime
N_s	: Number of events $B^0 \to \pi_B^+ X (D^0\pi_D^-)_{D^*}$, $B^+ \to \pi_B^+ X (D^0\pi_D^-)_{D^*}$
N_b	: Number of background events. A constraint on this parameter comes from chapter one: $< N_b >= 49.3 \pm 7.7$.
r_+	: relative amount of B^+ background, constrained to $< r_+ >= 8.9 \pm 5.4\%$.
r_b, τ_{b1}, τ_{b2}	: parameters to describe the background time spectrum.
τ_+	: the effective lifetime for the B^+ background ($< \tau_+ >= 1.01 \pm 0.20\ ps$).

The Likelihood function is a product for the signal sample and the background sample:

$$\mathcal{L} = \mathcal{L}^{signal}(\tau;\ r_+, N_s, N_b, r_b, \tau_{b1}, \tau_{b2}, \tau_+) \cdot \mathcal{L}^{backg}(r_b, \tau_{b1}, \tau_{b2}) \tag{2.9}$$

The likelihood for the signal part is given by:

$$\mathcal{L}^{signal} = e^{\frac{(N_b - <N_b>)^2}{2\sigma_{N_b}^2}} \cdot e^{\frac{(r_+ - <r_+>)^2}{2\sigma_{r_+}^2}} e^{\frac{(\tau_+ - <\tau_+>)^2}{2\sigma_{\tau_+}^2}} e^{-N_s - N_b} \cdot \prod_{i}^{\substack{signal \\ sample}} \mathcal{P}_i \tag{2.10}$$

with

$$\mathcal{P} = N_s\left[(1 - r_+)f_s + r_+ f_+\right] + N_b f_b \tag{2.11}$$

The functions f_s, f_b and f_+ were already defined in the previous section. The parameters for the background function are mainly determined from the likelihood function for the background sample:

$$\mathcal{L}^{backg} = \prod_{i}^{\substack{background \\ sample}} f_{b,i} \tag{2.12}$$

The result of the fit is shown in figure 2.5. The values obtained for the fit parameters are listed in table 2.1. The lifetime was determined to be

$$\boxed{\tau_{B^0} = 1.61\ ^{+0.22}_{-0.19}\ ^{+0.09}_{-0.07}\ ps} \tag{2.13}$$

The second error is the systematic error. The contributions to this error can be found in table 2.2 and were obtained in the following way:

- Momentum and decay length resolution

- The error on the decay length resolution was varied by $\pm 50\%$.
- The mean $< \ell_t - \ell >$ was changed by $\pm 50\ \mu m$.
- The resolution functions R^p, R^ℓ were parametrized by one gaussian instead of two.

- Fragmentation function
  The fragmentation parameter $\epsilon_b = 0.0032 \pm 0.0015$ was varied within the error.

- Efficiency
  - The statistical error for the efficiency functions was taken into account.
  - $\epsilon(\ell_t)$ was parametrized by a function $\epsilon(\ell_t) = a \arctan(b \cdot \ell_t)$ instead of $\epsilon(\ell_t) = a(1 + b/(1 + c \cdot \ell_t))$.
  - The effect of the signal composition was studied by enhancing or reducing the $\pi, \rho D^{*-}$ contributions by a factor of 2. No polarization was assumed in a second test.

- Background time distribution
  The test that the background sample shows the same time behavior as the real background (see figure 2.4) is limited by statistics. The distributions in figure 2.4 are all compatible with a constant ratio. The function f_b was modified for the signal likelihood $f_b \rightarrow a(1 + b \cdot \ell_t) \cdot f_b$ where the slope b was varied in the range $b = \pm 0.07$ obtained from the figures in 2.4.

- Integration of $G(t, t_t)$
  The integration of $G(t, t_t)$ was done numerically. The number of points used in the integration was changed by a factor of 18.

2.3 Conclusions

A new method was used to reconstruct B^0 mesons. The number of partial reconstructed hadronic B^0 decays, found in the 91-93 data, is about twice the number of full reconstructed B^0 at ALEPH [29]. The B^0 lifetime, obtained using these events, is compared with previous ALPEH measurements in the following table:

τ_{B^0}	total error	
$1.61\ ^{+0.22\ +0.09}_{-0.19\ -0.07}\ ps$	$^{+15}_{-13}$ %	this measurement
$1.71\ ^{+0.12\ +0.06}_{-0.11\ -0.06}\ ps$	$^{+8}_{-7}$ %	semileptonic decays[31]
$1.17\ ^{+0.24}_{-0.19} \pm 0.05\ ps$	$^{+21}_{-17}$ %	full reconstructed decays [29]

As long as the total errors are dominated by statistics, analyses based on semileptonic decays give the best results. With additional data (1994/1995) or when measurements from different experiments are averaged the method of partial reconstruction of hadronic decays will become important since the systematic errors are almost independent for the different methods.

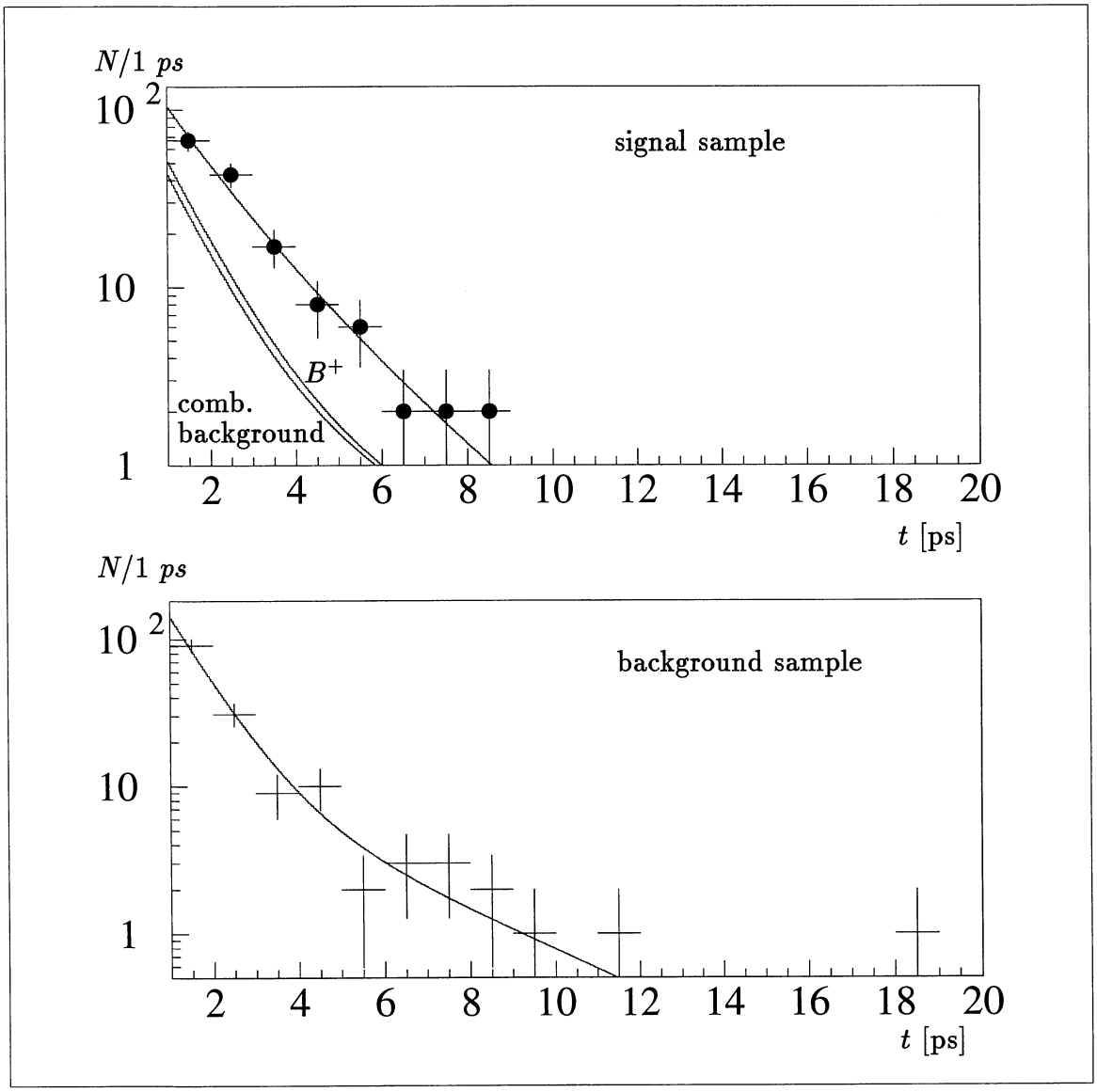

Figure 2.5: Fit results for the signal and the background sample. For the signal sample the background contribution and the contribution from $B^+ \to \pi^+ X D^{*-}$ decays are plotted as well.

	correlation coefficients							
	τ	N_s	N_b	r_b	τ_{b1}	τ_{b2}	r_+	$\tau+$
$\tau = 1.61^{+0.22}_{-0.19}$	1.000	-0.077	0.081	0.159	0.056	-0.077	0.139	-0.043
$N_s = 102 \pm 14$		1.000	-0.519	-0.031	-0.083	-0.009	0.002	0.000
$N_b = 47.1 \pm 7.7$			1.000	0.033	0.088	0.009	-0.002	0.000
$r_b = 0.75^{+0.13}_{-0.17}$				1.000	0.800	-0.852	0.001	-0.005
$\tau_{b1} = 0.88 \pm 0.19\ ps$					1.000	-0.653	0.013	-0.012
$\tau_{b2} = 3.31^{+1.81}_{-0.84}\ ps$						1.000	0.000	0.002
$r_+ = 0.083 \pm 0.054$							1.000	0.071
$\tau_+ = 1.03 \pm 0.17\ ps$								1.00

Table 2.1: Fit results

systematic error	
momentum spectrum	$^{+0.004}_{-0.006}\ ps$
background spectrum	$^{+0.078}_{-0.054}\ ps$
efficiency MC statistics	$^{+0.030}_{-0.045}\ ps$
efficiency systematics	$^{+0.035}_{-0.017}\ ps$
resolution function	$^{+0.018}_{-0.016}\ ps$
numerical integration	$\pm 0.010\ ps$
sum	$^{+0.093}_{-0.075}\ ps$

Table 2.2: Systematic uncertainties.

Appendix A

Monte Carlo simulation of $B \rightarrow \pi^+ X D^{*-}$ decays

The Monte Carlo simulation is based on the HVFL03 decay tables. Corrections were made to be in agreement with measurements on branching ratios and polarization (see table A.1,1.1). For all decays not included in table A.1 a D^{*-} polarization of $\Gamma_l/\Gamma = 54\%$ was assumed[30]. Branching ratios for D^{**} mesons can be found in table A.2,A.3 and A.4.

Decay	BR	Γ_l/Γ
$B^0 \rightarrow \pi^+ D^{*-}$	0.27 %	100 %
$B^0 \rightarrow \rho^+ D^{*-}$	0.72 %	93 %
$B^0 \rightarrow a_1^+ D^{*-}$	1.28 %	54 %
$B^0 \rightarrow (\pi^+\pi^0)_{non\ resonant} D^{*-}$	0.56%	93 %
$B^0 \rightarrow (\rho^0\pi^+)_{non\ resonant} D^{*-}$	0.68%	54 %
$B^0 \rightarrow \pi^- D_1^{*+}(2490)$	0.05%	100 %
$B^0 \rightarrow \pi^- D_1^{*+}(2422)$	0.11%	100 %
$B^0 \rightarrow \pi^- D_2^{*+}(2459)$	0.14%	100 %
$B^0 \rightarrow \rho^- D_1^{*+}(2490)$	0.13%	100 %
$B^0 \rightarrow \rho^- D_1^{*+}(2422)$	0.26%	100 %
$B^0 \rightarrow \rho^- D_2^{*+}(2459)$	0.27%	100 %
$B^- \rightarrow \pi^- D_1^{*0}(2490)$	0.18%	100 %
$B^- \rightarrow \pi^- D_1^{*0}(2422)$	0.11%	100 %
$B^- \rightarrow \pi^- D_2^{*0}(2459)$	0.14%	100 %
$B^- \rightarrow \rho^- D_1^{*0}(2490)$	0.26%	100 %
$B^- \rightarrow \rho^- D_1^{*0}(2422)$	0.26%	100 %
$B^- \rightarrow \rho^- D_2^{*0}(2459)$	0.27%	100 %

Table A.1: Monte Carlo branching ratios for hadronic B decays.

State	J^{PC}	mass [MeV]	width [MeV]	decay channels		reference
D_0^*	0^{++}	≈ 2400	≈ 250	$\to D^+\pi^-$	67 %	[16, 17],[18]
				$\to D^0\pi^0$	33 %	
D_1^*	1^{++}	≈ 2490	≈ 250	$\to D^{*+}\pi^-$	66 %	[16, 17],[18]
				$\to D^{*0}\pi^0$	33 %	
$D_1^*(2422)$	1^{+-}	2422 ± 2	21 ± 5	$\to D^{*+}\pi^-$	53 %	[21, 19, 22, 23, 24],[18]
				$\to D^{*0}\pi^0$	27 %	
				$\to D^+\pi^-\pi^0$	10 %	
				$\to D^0\pi^-\pi^+$	10 %	
$D_2^*(2459)$	2^{++}	2459 ± 2	22 ± 5	$\to D^+\pi^-$	43 %	[21, 20, 22, 23, 24],[18]
				$\to D^0\pi^0$	22 %	
				$\to D^{*+}\pi^-$	17 %	
				$\to D^{*0}\pi^0$	8 %	
				$\to D^{*+}\pi^-\pi^0$	5 %	
				$\to D^{*0}\pi^-\pi^+$	5 %	

Table A.2: Properties of the four $L = 1$ excited D mesons.

Decay	$\frac{BR(B^- \to D_J^{*0}\pi^-,\rho^-)}{BR(B \to D^{*0}(2420)\pi^-)}$				reference
	$D_0^*(2400)$	$D_1^*(2400)$	$D_1^*(2422)$	$D_2^*(2459)$	
$B^- \to D_J^{*0}\pi^-$	2.3	1.7	1.	1.3	[25]
$B^- \to D_J^{*0}\rho^-$	2.9	2.4	2.4	2.5	[25]
$B^0 \to D_J^{*+}\pi^-$	0.4	0.5	1.	1.3	[25]
$B^0 \to D_J^{*+}\rho^-$	1.0	1.2	2.4	2.5	[25]

Table A.3: Predictions for the relative decay widths of $B \to D^{**}\pi, \rho$ decays.

Decay	$\frac{BR(B^- \to (D^{*+}\pi)\pi^-,\rho^-)}{BR(B^- \to D^{*0}(2420)\pi^- \to D^{*+}\pi^-\pi^-)}$ $D_1^*(2400)$	$D_1^*(2422)$	$D_2^*(2459)$	sum	reference
$B^- \to (D^{*+}\pi^-)\pi^-$	2.1	1	0.4	3.5	[25]
$B^- \to (D^{*+}\pi^-)\pi^-$	0.4	1.	0.3	1.7	[26]
$B^- \to (D^{*+}\pi^-)\rho^-$	3.0	2.4	0.8	6.2	[25]
$B^- \to (D^{*+}\pi^-)\rho^-$	0.9	1.9	0.6	3.4	[26]
$B^0 \to (D^{*+}\pi^0)\pi^-$	0.3	0.5	0.2	1.0	[25]
$B^0 \to (D^{*+}\pi^0)\pi^-$	0.2	0.5	0.1	0.8	[26]
$B^0 \to (D^{*+}\pi^0)\rho^-$	0.8	1.2	0.4	2.4	[25]
$B^0 \to (D^{*+}\pi^0)\rho^-$	0.4	1.0	0.3	1.7	[26]

Table A.4: Predictions for the relative decay widths of $B \to (D^{*-}\pi)\pi, \rho$ decays produced via $B \to D^{**}\pi, \rho$.

Decay	Branching Ratios [%] $D_1^*(2490)$	$D_1^*(2422)$	$D_2^*(2459)$
$B^- \to D_J^{*0}\pi^-$	0.18	0.11	0.14
$B^- \to D_J^{*0}\rho^-$	0.26	0.26	0.27
$B^0 \to D_J^{*+}\pi^-$	0.05	0.11	0.14
$B^0 \to D_J^{*+}\rho^-$	0.13	0.26	0.27

Table A.5: Branching ratios used for the simulation of $B \to D^{**}\pi, \rho$ decays. The values are normalized to the measured branching ratio $B^- \to \pi^-\pi^- D^{*+} = 0.20\%$.

Bibliography

[1] R.Giles *et al* (CLEO Collaboration), Phys. Rev. **D30** (1984) 2279.

[2] A.Albrecht *et al* (ARGUS Collaboration), Phys. Lett. **B182** (1986) 95.

[3] A.Albrecht *et al* (ARGUS Collaboration), Phys. Lett. **B342** (1994) 249.

[4] S. Abachi *et al* (HRS Collaboration), Phys. Lett. **B205** (1988) 411.

[5] D. Decamp *et al* (ALEPH Collaboration), Phys. Lett. **B266** (1991) 218.

[6] A.Albrecht *et al* (ARGUS Collaboration), DESY 94-094 (1994).

[7] M. Athanas *et al* (CLEO Collaboration), CLNS 94/1286 (1994).

[8] R. Enomoto *et al* (TOPAZ Collaboration), KEK 93-215 (1993).

[9] A.Albrecht *et al* (ARGUS Collaboration), DESY 90-157 (1990).

[10] T. Hamacher (ARGUS Collaboration), Doctoral Thesis, DESY-F15-93-05.

[11] M.S. Alam *et al* (CLEO Collaboration), CLNS 94/1270 (1994).

[12] Review of Particle Properties, Phys. Rev. **D45** (1992). Branching ratios are scaled using $BR(D^{*+} \to D^0\pi^+) = 0.68\%$.

[13] C. Bebek *et al* (CLEO Collaboration), Phys. Rev. **D36** (1987) 1289.

[14] A.Albrecht *et al* (ARGUS Collaboration), Z. Phys. **C48** (1990) 543. Branching ratios are scaled using $BR(D^{*+} \to D^0\pi^+) = 0.68\%$.

[15] Bortoletto *et al* (CLEO Collaboration), Phys. Rev. **D45** (1992) 21.

[16] S. Godfrey, N. Isgur, Phys. Rev. **D32** (1985) 189.

[17] S. Godfrey, R. Kokoski, Phys. Rev. **D43** (1991) 1679.

[18] A.F. Falk, M. Luke,, Phys. Lett. **B292** (1992) 119.

[19] A.Albrecht *et al* (ARGUS Collaboration), Phys. Lett. **B232** (1989) 398.

[20] A.Albrecht *et al* (ARGUS Collaboration), Phys. Lett. **B221** (1989) 422.

[21] J.C. Anjos *et al* (E691 Collaboration), Phys. Rev. Lett. **62** (1989) 1717.

[22] P. Avery *et al* (CLEO Collaboration), Phys. Rev. **D41** (1990) 774.

[23] P.L. Frabetti *et al* (E687 Collaboration), Phys. Rev. Lett. **72** (1994) 324.

[24] P. Avery *et al* (CLEO Collaboration), CLNS 94/1280 (1994).

[25] P. Colangelo, F. De Fazio, G. Nardulli, Phys. Lett. **B303** (1993) 152. a_1 *and* a_2 *were set to* 1.15 *and* 0.26, *respectively [24].*

[26] C. Reader, N. Isgur, Phys. Rev. **D47** (1993) 1007.

[27] D. Buskulic *et al* (ALEPH Collaboration), Z. Phys. **C62** (1994) 179.

[28] R. Forty , CERN-PPE/94-144.

[29] D. Calvet, J. Carr (ALEPH Collaboration), ALEPH 94-100.

[30] H. Kuipers (ARGUS Collaboration), *diploma thesis*, DESY F15-91-04 (1991).

[31] ALEPH Collaboration, *Measurement of the* $\overline{B}^0$ *and* B^- *Meson Lifetime*, Contribution to the 27th International Conference on High Energy Physics, Glasgow (1994).